NTNU – Trondheim
Norwegian University of
Science and Technology

Numerical Investigation of Free Surface Flows

Silas Spence

Marine Technology
Submission date: June 2014
Supervisor: Bjørnar Pettersen, IMT
Co-supervisor: Håvard Holm, IMT
Vladimir Krasilnikov, MARINTEK

Norwegian University of Science and Technology
Department of Marine Technology

Abstract

The Star-CCM+ simulation software has been used to model a number of benchmark free surface flow cases, including the two dimensional submerged NACA 0012 foil, the surface piercing NACA 0024 foil, and the well investigated KCS vessel. The findings from the foil benchmark cases have permitted substantial improvement in the accuracy and convergence of the results for the KCS vessel when compared to preliminary studies undertaken as part of the master's project.

It has been observed that a minimum set of temporal and spatial resolutions are required to yield an acceptable numerical solution, and guidelines to ensure that these requirements are met have been formulated, including modification of the default Star-CCM+ solver parameters for supposedly steady state free surface flows. Time step independent solutions for all of the cases investigated have been found, however the mesh resolution requirements to obtain this independence vary significantly, and some practical limitations regarding mesh size in the ship case precludes taking the most demanding requirements found and using them as a general recommendation. Some additional work, focusing on investigation of additional ship cases, has been proposed with the objective of clarifying guidelines for creating a time step independent mesh for ship flow problems.

In general, a modelling approach has been identified using the Star-CCM+ software which yields a satisfactory result for a ship resistance prediction and a good starting point for further investigation of the nominal wake scaling problem.

NTNU
Det skapende universitet

MASTERKONTRAKT
- uttak av masteroppgave

1. Studentens personalia

Etternavn, fornavn **Spence, Silas**	Fødselsdato **27. aug 1982**
E-post **spence@stud.ntnu.no**	Telefon **41350455**

2. Studieopplysninger

Fakultet **Fakultet for ingeniørvitenskap og teknologi**	
Institutt **Institutt for marin teknikk**	
Studieprogram **Marine Technology**	Studieretning **Marine Hydrodynamics**

3. Masteroppgave

Oppstartsdato **03. feb 2014**	Innleveringsfrist **30. jun 2014**
Oppgavens (foreløpige) tittel **Numerical Investigation of Flow Around Unappended Ship Hull**	
Oppgavetekst/Problembeskrivelse The candidate shall conduct numerical investigations of the unappended KCS and, if time permits, the KVLCC hull forms at both model scale and full scale using the Star-CCM+ commercial software package. Intermediate scales may be investigated if deemed necessary. The model scale numerical results shall be benchmarked against published experimental and numerical data. Prior to the scaling investigation, efforts to improve the simulation results at model scale shall be undertaken through theoretical and practical means, with free surface and turbulence modelling as areas of primary interest. The full scale nominal wake results shall be compared with at least the ITTC wake fraction scaling method. If time permits, and it is deemed useful, comparison with empirical scaling methods may be expanded to include Yazaki's method (1969), and possibly the Sasajima-Tanaka Method.	
Hovedveileder ved institutt **Professor Bjørnar Pettersen**	Medveileder(e) ved institutt **Håvard Holm**
Ekstern bedrift/institusjon **MARINTEK**	Ekstern veileder ved bedrift/instutisjon **Vladimir Krasilnikov**
Merknader **1 uke ekstra p.g.a påske.**	

Preface

The work presented in this thesis has been undertaken in conjunction with the PROPSCALE competence building project, consisting of a consortium of industrial and research partners with support from the Norwegian Research Council, which is being coordinated by MARINTEK and runs from 2013 until 2016.

The purpose of the PROPSCALE project is twofold; the scale effects on ship and propulsor characteristics are to be investigated, placing emphasis on podded and ducted propulsors (though single screw vessels are also an important part of the project scope), with the ultimate goal of improved performance predictions from numerical and model scale experimental results, and to provide a set of practical methods and tools for CFD analysis of ship resistance and propulsion, primarily for the benefit of the industrial partners.

Within this framework, the basic areas of focus break down into the following categories:

- Ship nominal wake (based on towing experiments) and scaling of these results
- Propulsor performance under open water conditions
- Ship-propulsor interaction

The tool used throughout the PROPSCALE project is the Star-CCM+ software package from CD-Adapco. This was driven by the preferences of the of the project partners, and was further strengthened by having CD-Adapco participate in the project.

The intent of this master's thesis, as outlined in the master's contract, was to investigate the first point: scaling of ship nominal wake. In the course of preliminary studies, undertaken as part of the masters project, a number of issues were encountered with the simulations, mainly relating to the numerical modelling of the free surface flow around the ship hull. An adequate solution of the free surface flow is of crucial importance for accurate prediction of the vessel wave resistance and has a significant influence on the pressure distribution over the hull, which in the stern region may directly influence the development of the nominal wake behind the hull. Thus, it was deemed a prerequisite to the nominal wake scaling investigation to address the free surface modelling problem in more detail through a systematic series simulations with benchmark cases, including two and three dimensional foils as well as a ship hull, where available experimental data permitted a thorough assessment of the numerical method, the results of which are presented in this thesis. As such, this work does not directly address the nominal wake scaling problem, but it does provide a good foundation from which to proceed with such investigations, as well as contributing to the practical CFD guidelines, which are one of the deliverables of the PROPSCALE project.

Acknowledgment

I would like to thank my supervisor, Håvard Holm, and co-supervisor, Vladimir Krasilnikov, for their time, patience, and guidance in undertaking the work presented in this thesis. In addition, I would like to thank all the partners involved in the PROPSCALE competence building project (listed below) and the Norwegian Research Council for providing the infrastructure within which I have had the opportunity to conduct my master's thesis. The help and support of the Ship Technology Department at MARINTEK must also be acknowledged, not in the least for the use of the **nise** computing cluster, with special thanks to Kourosh Koushan, Anders Östman, and Luca Savio.

- MARINTEK – Norwegian Marine Technology Research Institute
- NTNU – Norwegian University of Science and Technology
- HiÅ – Ålesund University College
- TUHH – Technical University of Hamburg-Harburg
- CSSRC – China Ship Scientific Research Center
- Havyard Group AS
- Rolls-Royce Marine AS
- Scana Volda AS
- VARD Design AS
- CD-Adapco

Silas Spence

Contents

List of Figures

List of Tables

Nomenclature

Δt	time step
λ	Wavelength
μ_τ	Friction velocity, given as $\mu_\tau = \sqrt{\frac{\tau_w}{\rho}}$
ν	Kinematic viscosity
ρ	Density
τ_w	Wall shear stress
ϕ	Displacement function used in the Level Set method
2D	Two dimensional
3D	Three dimensional
c	Volume fraction, as used in the Volume of Fluid method
$\tilde{c_C}$	normalized cell value for volume of fluid
C_D	drag coefficient
C_f	Skin friction coefficient
$\tilde{c_j}$	normalized cell face value
$\tilde{c_j^*}$	Courant number corrected normalized cell face value
C_p	Pressure coefficient
CFD	Computation Fluid Dynamics
Co	Courant number
Cu_h	Upper Courant number limit in the Star-CCM+ VOF solver
Cu_l	Lower Courant number limit in the Star-CCM+ VOF solver
Fr	Froude number
GB	Gigabyte
GHz	Gigahertz
HRIC	High Resolution Interface Capturing scheme
ITTC	International Towing Tank Conference

KCS	KRISO Container Ship
KRISO	Korea Research Institute of Ships & Ocean Engineering, now known as the Maritime & Ocean Engineering Research Institute (MOERI)
QDR	Quad data rate
RANS	Reynolds-averaged Navier–Stokes equations
Re	Reynolds number
SIMPLE	Semi-Implicit Method for Pressure Linked Equations
$TFLOPS$	A unit of computational speed, indicating a rate of one trillion floating point operations per second (FLOPS)
L	Characteristic length
L_{PP}	length between perpendiculars
MARINTEK	The Norwegian Marine Technology Research Institute
NACA	National Advisory Committee for Aeronautics
VOF	Volume of Fluid
y^+	Dimensionless wall distance, defined as $y^+ = \frac{y\mu_\tau}{\nu}$

Chapter 1

Introduction

This thesis presents a systematic investigation into the numerical modelling of free surface flows, such as those found around a ship, using the Star-CCM+ computational fluid dynamics (CFD) software package. The motivation for this stems from issues encountered during preliminary work, undertaken within the framework of the masters project, with simulating the flow around the KRISO Container Ship (KCS). The nature of these issues, which are expanded upon in greater detail in Section 1.1, led to the following objectives for this thesis work:

- Gain a better understanding of free surface modelling methods in CFD and identify the relevant parameters and parameter values prerequisite to obtaining acceptable results for such problems with the Star-CCM+ software package.
- Apply this understanding and knowledge to the simulation of the KCS vessel and evaluate whether or not the revised approach yields a solution that is a good end point for a typical fixed trim towing test and a good starting point for further investigations into the wake scaling problem.

The first objective has been realized through a literature review on the subject of numerical free surface modelling, which is summarised in Chapter 2, and through the investigation of the classic two dimensional submerged NACA 0012 foil (Chapter 4) and the surface piercing NACA 0024 foil (Chapter 5). These cases offer good reference experimental data against which the simulations are benchmarked. During these test cases, the primary focus was on:

1. Achieving time step independent numerical solutions, in terms of drag coefficient and wave elevation, for the supposedly steady-state problems.
2. Improving convergence of the solution residuals, as an indicator of quality of the CFD simulation and reliability of the results.

The application of the findings from the foil test cases to the KCS vessel is presented in Chapter 6. A summary and assessment of the findings, in keeping with the second objective stated above, is presented in Chapter 7.

The numerical results presented in this thesis were obtained using the **nise** computing cluster at the Ship Technology Department of MARINTEK. This cluster is composed of 16 compute nodes, each of which contains a pair of Intel hexacore processors (E5-2620) running at

2.0 GHz with 64 GB of memory, connected via a low latency QDR Infiniband network, for a total of 192 compute cores and a theoretical peak performance of 3.07 $TFLOPS$.

1.1 Inital KCS Vessel Results

The objective of the simulations undertaken as part of the masters project was to obtain a converged solution for the case of the KRISO Container Ship at model scale, in calm water and with fixed heave and trim; essentially replicating the towing tests conducted by the Korean Maritime and Ocean Engineering Research Institute (Kim et al., 2001). This was completed successfully, using a fairly simple meshing approach and mainly default settings within Star-CCM+. In spite of the generally satisfactory agreement between the experimental and numerical results, the numerical results obtained did raise two issues:

1. The residuals showed fairly poor convergence of only one to two orders of magnitude in the best cases, despite the drag coefficient showing quite good convergence at the same time.

2. The free surface elevations in the far field showed a marked time step dependency, and tended to converge to a larger amplitude than the experimental values. This dependency also appeared to influence the pressure component of the total vessel resistance, as it too showed a similar time step sensitivity.

The specifics of these issues are given in more detail in the following sections. As it was suspected that the residual convergence issues were linked to the free surface discretization, the efforts at improving the simulation results focus on the modelling and discretization of the free surface region.

1.1.1 Free Surface Time Dependency

As the KCS case represents what can essentially be considered a steady state problem, it is reasonable to expect that a time step independent problem setup can be found which converges to the expected (in this case experimental) solution. Thus, it is quite surprising to find that the Star-CCM+ solver, as configured in this case, shows both a strong sensitivity to time step, and also tends to a larger amplitude than the experimental results in the far field as the time step becomes sufficiently small, as shown in Figure 1.1 which compares time steps of 0.05s and 0.025s against experimental results for a longitudinal wave cut $y = -0.1509L_{PP}$ away from the vessel centerline. This behaviour has been reported for the KCS case, with Star-CCM+, by Krasilnikov (2013).

Clearly, it is highly desirable to find, if possible, a modelling approach within Star-CCM+ that provides the expected time step independency for the wave elevations in order to limit the number of relevant variables during further investigations, as well as improve the agreement between the experimental and numerical results.

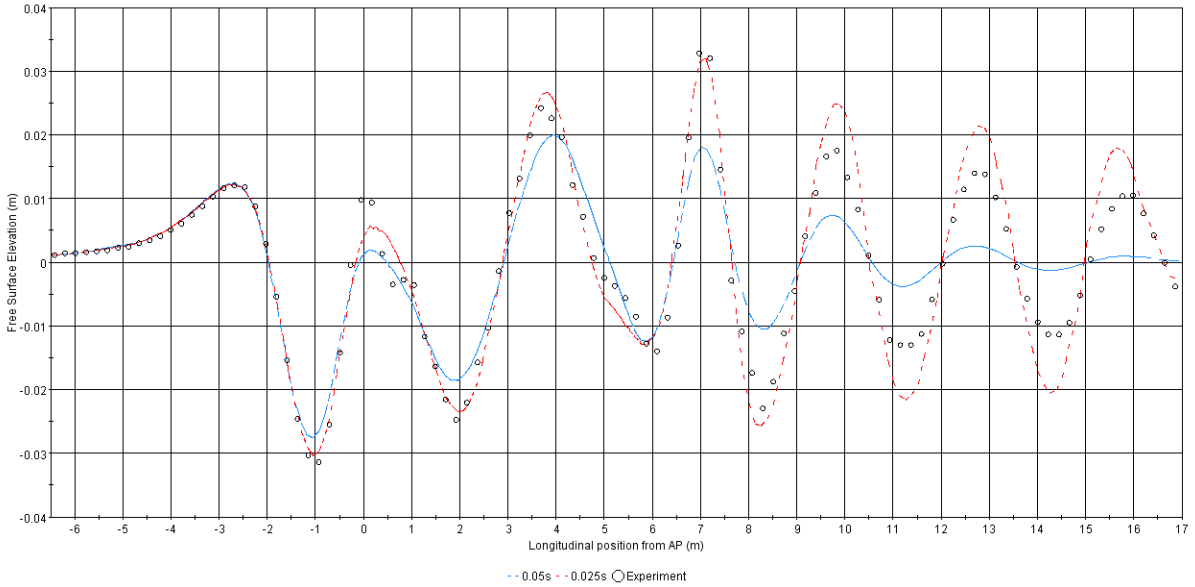

Figure 1.1: Sensivity of free surface elevation to time step, at 0.05 s and 0.025 s, in initial KCS simulations at a longitudinal cut $y = -0.1509L_{PP}$ off vessel centerline

1.1.2 Poor Residual Convergence

In the KCS case, where there is a wealth of experimental data from model towing tests, the poor residuals are not of overwhelming concern as data for drag, free surface elevations both on the ship hull and at various distances from the ship hull, and nominal wake measurements can be compared against the experimental data and the quality of the results assessed based on the convergence history of the force coefficients (such as drag) and agreement between the two data sources. While this does imply a strong assumption regarding the accuracy and quality of the experimental data, this is nonetheless common practice when evaluating results from numerical simulations. However, when attempting to take the modelling approach used in this case and generalize its application to other cases, such as the KCS vessel at full scale, or other similar single screw vessels, where little or no reference data is available, the quality of the simulation is largely gauged by the convergence of the residuals and force coefficients both within a single simulation, and over a typical grid dependence study. In the face of poor residual behaviour and limited reference data, it can become very difficult to assess the reliability of the results obtained in such circumstances, making it a clear advantage to pursue improved numerical behaviour of the solution through alternate modelling and problem setup, if possible. A representative example of the residuals obtained during the project work with the KCS case is shown in Figure 1.2, where it can be seen that the residuals show a large amount of high frequency noise and overall convergence of only 1-2 orders of magnitude.

It has been noted by a number of Star-CCM+ users at MARINTEK that this kind of residual behaviour is not unusual, at least for free surface flows, and the normal work around is focusing on the convergence behaviour of the relevant force coefficients for the problem instead. While this will facilitate assessing aspects such as adequate simulation duration and grid convergence, it still remains more difficult to be confident that the numerical solution is converging to a physically meaningful solution if the residuals, with some additional emphasis on the momentum residuals, are not also showing good convergence, indicating that

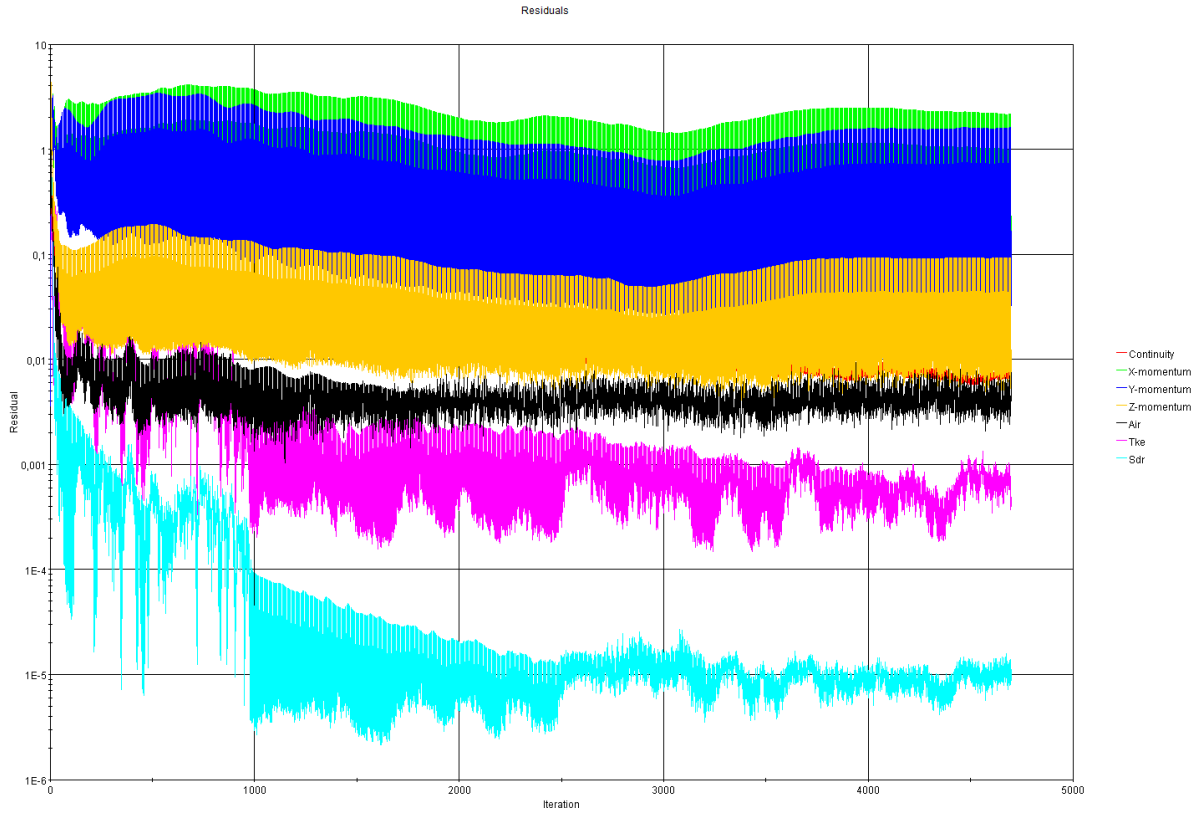

Figure 1.2: Residual plot of an initial KCS vessel simulation, showing poor normalized residual convergence, particularly of the momentum terms

the underlying numerics are struggling with some aspect of the flow problem.

Chapter 2

General CFD Discussion

The objective of this chapter is to provide an overview of some of the particularities of computational fluid dynamics (CFD) simulations of problems featuring a free surface, as well discuss some of the recommendations available to help obtain adequate results. Some degree of familiarity with CFD methods is assumed, as it is throughout the rest of this thesis.

The majority of current viscous flow simulation codes, including Star-CCM+, solve the Navier Stokes equations in discretized form, with the finite volume approach being the most common. The derivations for these approaches are found throughout the literature, including Ferziger and Perić (2002); Löhner (2008); Ransau (2004), and will not be replicated here.

It may be argued that the free surface is of secondary importance (compared to considerations such as turbulence models, for example) to the nominal wake problem. For the KCS vessel, at a moderate Froude number of 0.26, that may be the case. However, it is important to keep in mind that the work with the KCS vessel is a case study which will form a basic modelling approach that shall be applied to a larger test matrix of diverse hull forms. Separation can play a significant role in defining the nominal wake, particularly for blunter hull forms, and as reported by Zhang and Stern (1996), the free surface elevation near the body can play a significant role defining the separation region, even on a flat plate. In addition, at higher Froude numbers, the relative contribution of the wave component to the nominal wake field increases, possibly even coming to dominate it and generate a wake field with a negative sign in the some special cases such as high speed vessel and destroyers (Lewis et al., 1988). As a secondary consideration, the trade-offs of choices such as turbulence model, for example, must be assessed not only based on ability to resolve the nominal wake field, but also to deliver the correct drag coefficient. An effective assessment of this consideration requires that the free surface is well modelled in order to limit uncertainty when comparing with experimental results.

2.1 Free Surface Modelling

The modelling and solution of free surface flows pose some particular challenges. In the case of a ship simulation, with water and air as the flow phases, the density jumps by three orders of magnitude across a sharp interface that is capable of deforming in an arbitrary manner.

The free surface is characterised by two conditions; the kinematic and the dynamic free surface conditions (Faltinsen (1993)). Neglecting surface tension, which is typically a valid simplification for free surface flows around bodies such as ships if there is no cavitation or other significantly bubbly regions to the flow, the free surface boundary conditions can be given as follows: the kinematic free surface condition states that a particle on the free surface remains on the free surface, while the dynamic free surface condition is that the water pressure is equal to the atmospheric pressure at the free surface. Interface tracking and interface capturing are the two main categories of methods used to implement these conditions in CFD codes.

Interface tracking methods define the free surface as a sharp interface and follow its evolution over time. Typically, but not always, the mesh is fitted to the free surface, with the free surface treated as a boundary upon which the kinematic and dynamic conditions are enforced directly, and so must evolve with the free surface over time, requiring adaption of the mesh with each time step. Common interface tracking methods include:

- Height function method
- Line segment method

The height function method is the simplest and most computationally efficient approach, but cannot handle cases such as bubbles or breaking waves. The line segment method becomes extremely computationally demanding in 3D problems and as such is rarely used in such situations.

Interface capturing methods track a volume within a fixed domain which encompasses the free surface. Common implementations include:

- Marker-and-cell (MAC) technique
- Level set method
- Volume of fluid (VOF) approach

The marker-and-cell technique uses massless particles distributed throughout one of the fluid phases, and which are convected along with the flow, in order to locate the fluid volume and thus the free surface: cells with a marker and at least one neighbor without a marker are on the free surface. This technique is very simple and able to handle complex phenomena such as breaking waves and bubbles, but in a general 3D problem imposes high computational requirements due to the need to track a large number markers. In addition, the markers must be redistributed throughout the volume as velocity gradients will tend to create areas of high and low concentrations of markers over time.

The level set method solves a transport equation, given in Equation (2.1), where ϕ is the signed distance between a point and the free surface.

$$\frac{\partial \phi}{\partial t} + \nabla \cdot (\mathbf{u}\phi) = 0 \tag{2.1}$$

This method can handle cases such as breaking waves and droplets or bubbles. However, the level set function, ϕ, does require reinitialisation in order to ensure that it remains a distance function during the course of the computation. This reinitialisation step is an important source of error in the level set method.

The volume of fluid approach is one of the more commonly implemented methods in marine applications, featuring reasonable computational demands (typically higher than the height function approach, but lower than the MAC method) and the ability the handle breaking waves, droplets, and bubbles. The VOF approach introduces the function, c, which has a value of one when filled with fluid, and zero when empty: cells with a value of c between zero and one then contain the free surface. The free surface solution is obtained by solving Equation (2.2), which is of the same form as that of Equation (2.1) used in the level set method.

$$\frac{\partial c}{\partial t} + \nabla \cdot (\mathbf{u}c) = 0 \tag{2.2}$$

The choice of how to handle the two phase flow has some influence on how the kinematic and dynamic free surface conditions are implemented in the VOF method. In solving the flow equations for only the liquid phase, Hirt and Nichols (1981) use a pressure interpolation scheme to impose the free surface conditions at the correct boundary location, a necessary step as the free surface is normally not exactly co-located with the mesh grid points. Muzaferija and Peric (1999) take a different approach, treating both the air and water phases as a single fluid whose properties (density and viscosity) vary according the the concentration (volume fraction) of each phase found in each cell, as per Equation (2.3), where subscripts 1 and 2 denote the respective phases (water and air, for example). With this approach, the free surface is not a treated as a boundary and thus no there is no need to prescribe the free surface conditions on it; satisfying the kinematic free surface condition is implicit in the solution of Equation (2.2), while the dynamic condition is also implicitly taken into account (Ferziger and Perić (2002)).

$$\rho = \rho_1 c + \rho_2 (1 - c), \quad \mu = \mu_1 c + \mu_2 (1 - c) \tag{2.3}$$

With the VOF method, the free surface is represented by a discontinuity in the function, c, which requires some special care in handling the discretization of the convection term in Equation (2.2) in order to obtain a sharp interface. It is important to keep in mind that, with the VOF method, the value of c must be bounded in the range $0 \leq c \leq 1$. The first-order upwind scheme satisfies this boundedness criterion but smears the interface over a wide region due to artificial mixing of the phases. Higher order schemes, such as second order central differencing or Crank-Nicholson, tend to produce over- and undershoots in the vicinity of discontinuities (such as the free surface) due to not satisfying the boundedness criterion.

The High Resolution Interface Capturing (HRIC) scheme proposed by Muzaferija and Peric (1999) is an approach that aims to address the aforementioned issues with the convective term in Equation (2.2) by approximating the normalized cell face value, $\tilde{c_j}$, according to Equation (2.4), where $\tilde{c_C}$ is the normalized cell value for volume of fluid.

$$\tilde{c_j} = \begin{cases} \tilde{c_C} & \text{if } \tilde{c_C} < 0 \\ 2\tilde{c_C} & \text{if } 0 \leq \tilde{c_C} < 0.5 \\ 1 & \text{if } 0.5 \leq \tilde{c_C} < 1 \\ \tilde{c_C} & \text{if } 1 \leq \tilde{c_C} \end{cases} \tag{2.4}$$

The value of $\tilde{c_j}$ is then modified according to the availability criterion, which states that the amount of fluid convected across a cell face should not exceed the amount of fluid available within the donor cell, according to Equation (2.5). Co is the convective Courant number, as shown in Equation (2.6), where $v \cdot nS_j$ is the volumetric flow rate the through the j^{th} cell face, ΔV_C is the volume of the donor cell, and Δt is the time step.

$$\tilde{c_j^*} = \begin{cases} \tilde{c_j} & \text{if } Co < 0.3 \\ \tilde{c_C} + (\tilde{c_j} - \tilde{c_C})\frac{0.7-Co}{0.7-0.3} & \text{if } 0.3 \leq Co < 0.7 \\ \tilde{c_C} & \text{if } 0.7 \leq Co \end{cases} \tag{2.5}$$

$$Co = \frac{\mathbf{v} \cdot \mathbf{n} S_j \Delta t}{\Delta V_C} \tag{2.6}$$

The effect of the application of Equation (2.5) is that for regions with local Courant numbers below the lower threshold of 0.3, the HRIC discretization scheme is used, while for regions with local Courant numbers above the upper limit of 0.7, a purely upwind scheme is used, with regions falling in between using a blended scheme. The significance of the Courant number based correction of Equation (2.5) in the HRIC scheme is discussed further in Section 3.3 and Chapter 4.

For further reading, Ransau (2004) provides a good overview of free surface modelling approaches, while Ferziger and Perić (2002) goes into more detail and includes case studies.

2.2 Resolution Guidelines for Capturing Free Surfaces

The particulars and intricacies of mesh generation are well beyond the scope of this work and will not be discussed in detail. However, there are a number of sources of guidance available which can help reduce the time required to generate a mesh of good quality for a free surface problem. The International Towing Tank Conference (ITTC) has published Practical Guidelines for Ship CFD Application (ITTC, 2011), which provides a number of useful guidelines including a recommended minimum number of cells per wave amplitude and wavelength (see Table 2.1, and an equation (eq. (2.8)) for calculating a range for the time step for the simulation. While these guidelines can provide a useful starting point, it is not clear whether the basis of the mesh and time step resolution recommendations are theoretical or empirical in nature, and how applicable they are to the code used in this work, Star-CCM+.

Table 2.1: Comparison of CD-Adapco and ITTC free surface mesh resolution recommendations

	Cells per Wave Length	Cells per Wave Amplitude
CD-Adapco	80-100	20
ITTC	40	10

While a good starting point, the ITTC guidelines are not the only ones available; CD-Adapco has also issued a set of guidelines (Gillis), which give recommendations for the minimum

number of cells per wavelength and wave amplitude, as well as the time step. As can be seen from Table 2.1, the Star-CCM+ mesh resolution recommendations are essentially twice as demanding as the ITTC guidelines.

The equation given by CD-Adapco for the time step is given in Equation (2.7), while Equation (2.8) is from the ITTC guidelines. While the basis for the CD-Adapco guidelines (empirical vs theoretical) is again unclear, it is at least clear that these guidelines are intended for the CFD code in question.

$$\Delta t_{STAR} = \frac{\text{Wave Period}}{\text{Number of Cells per Wave Length} \times 2.4} \tag{2.7}$$

$$\Delta t_{ITTC} = 0.005 \sim 0.01 \frac{L}{U} \tag{2.8}$$

The characteristic length and velocity found in Equation (2.8) are not explicitly defined. For the purposes of this thesis, they are assumed to be the wavelength and wave propagation speed (which is equivalent to the vessel speed or mean free stream velocity for the cases considered here). Equations (2.7) and (2.8) can then be seen to be equivalent when the number of cells per wavelength is in the range of $42-84$. It is interesting to note that CD-Adapco recommends an approach where increasing mesh resolution is accompanied by increasing time step resolution, essentially applying some form of a Courant number requirement.

It is important to note that the guidelines presented in this section are restricted to the resolution of free surface waves; appendages or other aspects of the geometry in question may introduce flow features (separation, vortices, etc.) with different length or time scales than those relevant to the free surface and must be accounted for as well. In addition, the time step recommendations are only valid for an implicit temporal discretization scheme as they generally do not satisfy the stability requirements for an explicit scheme when taken in conjunction with the mesh resolution requirements given in Table 2.1.

2.2.1 Near-wall Modelling

Resolving the boundary layer near the surface of a body (wall) is typically a very important aspect of obtaining good simulation results. The two common approaches are to resolve the boundary layer using very high mesh resolution near the wall (fine near wall treatment), or to use wall functions (coarse near wall treatment), where a much larger distance from the wall to the first cell is used and the mesh resolution within the boundary layer is much lower. A detailed discussion of boundary layer theory can be found in White (1991), including a definition of the dimensionless wall distance, referred to as the y^+ value. For the fine near wall treatment, a target y^+ of 5 or less is desirable, while the target y^+ range for the coarse near wall treatment is typically $30-100$. For either treatment, the required first cell distance, y, corresponding to the target y^+ value can be estimated using Equation (2.9), as per ITTC (2011).

$$y = \frac{y^+}{Re\sqrt{\frac{C_f}{2}}} L_{PP} \tag{2.9}$$

Where the skin friction coefficient, C_f, is given by Equation (2.10).

$$C_f = \frac{0.075}{(log_{10}Re - 2)^2} \tag{2.10}$$

2.3 Convergence Criteria

Determining when a numerical solution has run for an adequate amount of time, or when the solution has "converged," is not always a straight forward task. Ideally, in a steady case, the residuals from the numerical solution methods will show a substantial drop, $3-4$ orders of magnitude according to the ITTC (2011) recommendations. Unfortunately, such ideal behaviour is not always observed, but this does not necessarily mean that the simulation results are poor.

Typically, in the absence of good residual convergence, increased emphasis is placed on the convergence of integral values such as force coefficients. General guidelines on what constitutes good convergence of a force coefficient are, apparently, very difficult to find, perhaps due to the difficulty in formulating them in a relevant yet generalized manner. In a purely steady case, such as the NACA 0012 case of Chapter 4, the force coefficients should display reducing oscillations until reaching a more or less stable value, usually with some very small but irregular variations about a mean value. However, the majority of flow problems around ships and and similar bodies are not truly steady; there is usually some amount of separated flow and/or unsteadiness in the wake. In such cases, the force coefficients may show a continuous "steady" oscillation, such as is shown in Figure 2.1. Fortunately, in many such cases, where the length and time scales necessary to capture the full extent of the unsteadiness in the flow are not adequately resolved, the oscillations tend to be very periodic in nature and eventually reach a consistent amplitude, making it fairly straightforward to obtain an accurate and meaningful average value. In the worst case, large regions of separation or instability exist in the flow, the time history of the force coefficients is erratic and subject to large amplitude variations, making an averaged value fairly meaningless.

In the work presented here, no extremely unsteady flows were investigated. In cases where the forces converged to an essentially stable value, the solution was deemed converged once the mean value ceased to vary significantly with time and the oscillation were within $2-3\%$ of the mean value. The mean value was then obtained from last suitable part of the simulation, typically over $4-8\,s$ of simulation time. For cases with larger stable oscillations in the force coefficients, the simulation was considered converged when the amplitude of the oscillation ceased to vary with time, with the mean value then being calculated from the last $8-10$ oscillations.

An important note regarding residuals as discussed in this section and throughout the rest of this work: these are normalized residuals, where the absolute value is normalized by some meaningful parameter, typically the maximum value of the same residual over the first $5-10$ iterations of the solution process.

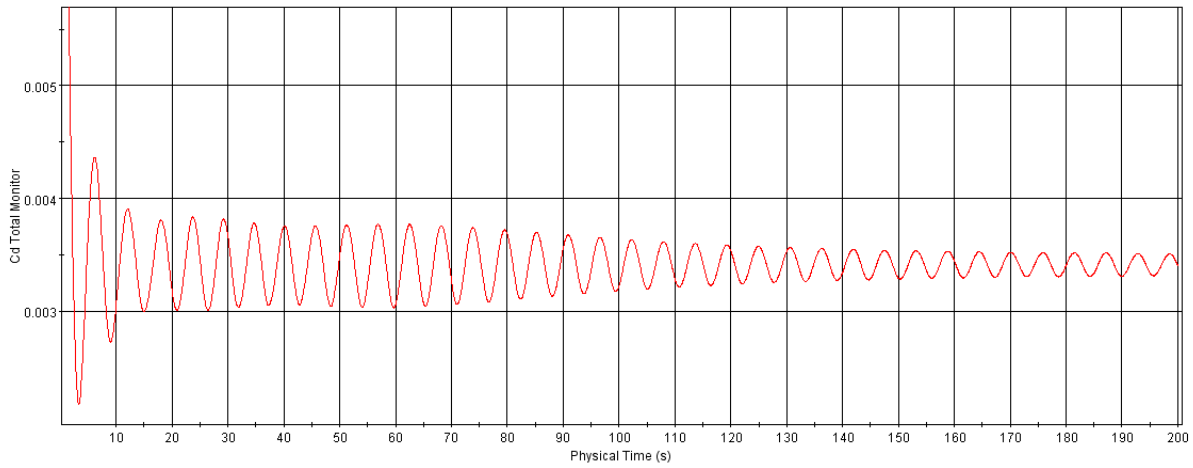

Figure 2.1: Convergence history of the drag coefficient for the KCS vessel at $Fr = 0.26$ for a 3.2 million cell mesh and a time step of 0.005 s

Chapter 3

Star-CCM+ Overview

Star-CCM+ is a commercial software code produced by CD-Adapco, originally released in 2004, and currently at version 9. As commercial software, the source code is proprietary and closed source. While the technical documentation is excellent, given the above constraint, this does leave the user in the position of needing to benchmark the code on reference cases that are representative of their intended use cases. Given the complex amalgamation of numerical mathematics, fluid dynamics, and computer science that is computation fluid dynamics, this benchmarking approach is often just as necessary with open source codes as few individuals have the requisite expertise in all of the aforementioned fields to assess the capabilities of a CFD program based solely on the source code. However, when discrepancies or anomalies are observed, the open source code does give the skilled user the possibility to delve into the source of observed issue, while proprietary codes leave the user wondering if the observed behaviour is due to modelling, setup, numeric methods, or an unresolved bug. The trade-off against such drawbacks are, compared with an option like OpenFOAM, a much more polished user interface and in depth software support.

There are a range of options provided by the Star-CCM+ software package for solving the Navier-Stokes equations. These include Reynolds Averaging (with a number of options for closure of the turbulent stress terms), Large Eddy Simulation (LES), Detached Eddy Simulation (DES), and inviscid potential flow. The work presented here utilizes the Reynolds Averaged Navier Stokes Equations approach (RANS). Further details about the options and choices made in this work for modelling free surface flows with Star-CCM+ are provided in the following sections of this chapter.

3.1 Meshing

The Star-CCM+ software package features an integrated meshing package which is capable of generating a number of different mesh topologies including:

- Trimmed hexahedral
- Polyhedral
- Tetrahedral
- Cylindrical

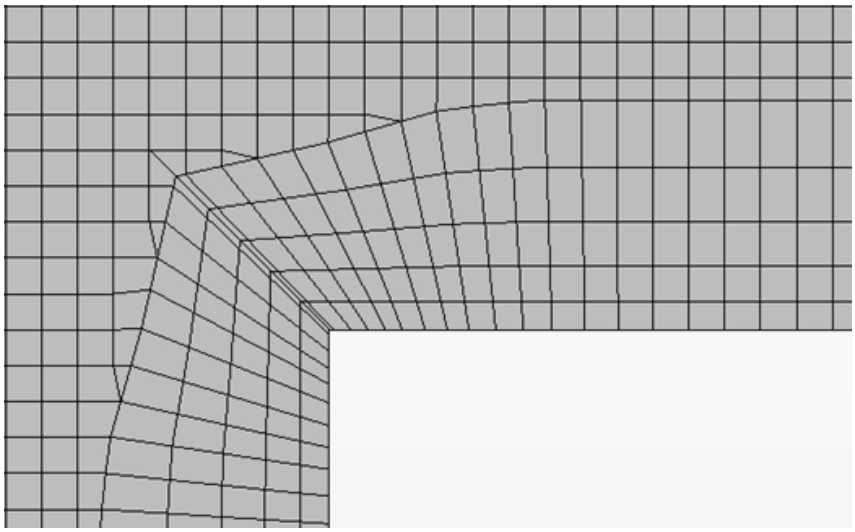

Figure 3.1: Sliver cells resulting from trimming of the volume mesh around the prism layer mesh

All of the meshes Star-CCM+ is capable of generating are, strictly speaking, unstructured as even fairly well structured topologies such as the hexahedral Trimmer mesher permit hanging nodes and accommodate irregular shapes via trimmed cells. Regardless of the volume meshing type selected, Star-CCM+ provides a single tool for resolving the boundary layer near no-slip walls: the prism layer mesher.

Local mesh refinements are implemented through user specified refinement volumes. These volumes can either be generated as basic primitives (quadrilaterals, cylinders, cones, etc) within Star-CCM+, or any arbitrary shape can be imported in suitable CAD format. Refinements to the volume mesh, or any surface intersecting the control volume, can be made either isotropically or anisotropically. The remainder of the meshing process is handled automatically. While this is extremely powerful and can potentially save a tremendous amount of time compared to more manual meshing approaches, it is not without some potential short comings which are discussed in the following subsection.

3.1.1 The Trimmer Mesher

The Trimmer mesher has been used exclusively in the work presented within this thesis. With its hexagonal cell topology and the ability of the trimmed cell approach to easily accommodate a wide range of arbitrary geometry, the resulting mesh is typically of high quality and presents high orthogonality to the mean free stream flow.

One practical point to note with the Trimmer mesher is that some combinations of geometry, volume mesh, and prism layer thickness may result in most of an outer volume cell being trimmed, with the resulting sliver causing a significant and undesirable jump in cell size (see Figure 3.1).

Also worth noting is that the Trimmer mesher, despite permitting hanging nodes, only allows for increasing or decreasing cell size by a factor of 2. This means that if a particular absolute value for the cell size is required in a certain region (such as ensuring adequate cells per wavelength around the free surface), the base size of the mesh must be a power of 2 of this

required cell size in order to actually realize the exact desired value. Otherwise, the cell size within region where the mesh refinement is applied will snap to the factor of 2 of the base size nearest to the input value. A consequence of this limitation is that cell aspect ratios will always be a power of 2 as well.

The mesh alignment option can improve sharpness of the free surface by aligning the undisturbed free surface to the edge of a row of mesh cells. This will normally result in a completely sharp interface between the air and water phases as the initial condition, and this sharpness will be retained in any areas of the domain where the surface remains undisturbed by waves. As with the prism layer mesher, it is possible to select a combination of domain size, mesh alignment, and base cell size which will result in sliver cells along a domain boundary where most of the cell is outside the domain and has thus been trimmed away, resulting in reduced mesh quality.

3.1.2 The Prism Layer Mesher

The purpose of this meshing tool is to resolve the boundary layer near surfaces upon which the no-slip flow condition has been imposed, which will create large velocity gradients in the direction normal to the surface. The prism layer mesher creates a temporary surface offset from the actual no-slip surface by the boundary layer thickness value set by the user, the volume mesh is then generated and trimmed to this temporary offset surface with the resulting temporary surface mesh extruded up to the target surface in a series of prismatic cells. The number of cells, the thickness of the cell nearest the wall, and the expansion rate of the prism cell thickness can all be adjusted in order to obtain the desired boundary layer resolution and y^+ values (depending on whether wall functions are to be used or not), as well as a smooth transition to the outer volume mesh.

Throughout this thesis work, a coarse wall treatment approach is used in order to limit computational demands, with the target y^+ value selected to be 50 and the associated first cell thickness calculated on a case-by-case basis according to Equation (2.9). The first cell thickness is a constant that is applied over the entire surface. For any geometry other than a flat plat, the near field flow velocity will vary substantially over the body, leading to variations in wall shear stress and thus, for a given first cell thickness, variations in the y^+ value. Conventional wisdom states that, when using wall functions, the first mesh point in the boundary layer should fall in the logarithmic region of the boundary layer, which is approximately $30 < y^+ < 100$ (Ferziger and Perić, 2002). While Star-CCM+ features the *All* y^+ wall function option, which claims to be able to handle a wide range of y^+ values, from one to over one hundred, there is little reason to deviate from this conventional wisdom. Enger et al. (2010) report good results for the KCS case with Star-CCM+ using a target y^+ of 50 and, as shown in Figure 3.2, using a target of 50 with the KCS case at $Fr = 0.26$ results in y^+ values in the range of $30 - 100$ over the majority of the hull, with only a small region around the skeg at the aft end dipping below 30.

3.2 Turbulence Modelling

Within the RANS solution approach to the Navier-Stokes equations, Star-CCM+ offers a wide variety of turbulence modelling options, including:

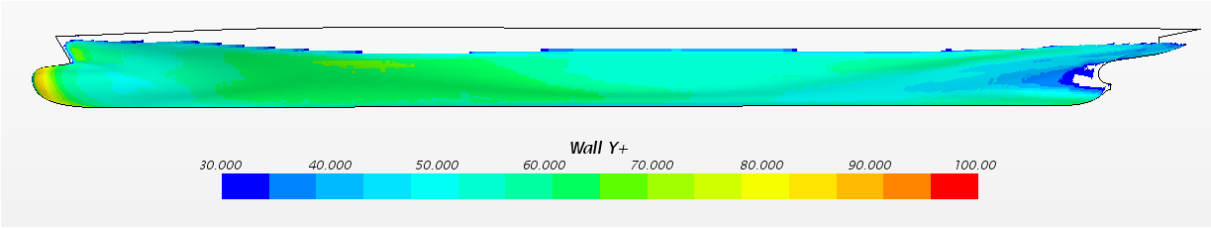

Figure 3.2: y^+ range over the KCS hull at $Fr = 0.26$

- Spalart-Allmaras
- k-ϵ
- k-ω
- Reynolds Stress Transport

The above list details only the general types; each model typically has multiple implementations. These models all have varying strengths, weaknesses, and computational demands.

For this thesis work, where the main focus is on modelling and resolving the free surface, the main objective with the turbulence model is to select one that is expected to provide adequate performance without excessive computational demands. To that end, the k-ω SST model of Menter (1994) has been selected. As a so-called two equation turbulence model, the computational demands are reasonable and good results with the KCS case have been reported by Enger et al. (2010); Krasilnikov (2013).

According to Menter, the k-ω SST model is intended to handle adverse pressure gradients and separation better than other two equation turbulence models. While considerations such as separation and adverse pressure gradients are not specifically of particular interest to the main focus of this work, within the larger scope of the PROPSCALE project such considerations become very significant in modelling nominal wake and hull-propulsor interaction correctly, so it again makes sense to begin with a model that is expected to be of use in future work.

The default Star-CCM+ parameters for the k-ω SST model were used without modification.

3.3 Free Surface Modelling

Star-CCM+ uses the Volume of Fluid model exclusively for free surface flows. In this model, the various fluid phases are assumed to be immiscible and all phases share velocity and pressure fields (the fluids are modelled as one flow, with varying properties according to Equation (2.3). This VOF model is a segregated flow model, with the pressure and velocity fields coupled using an implementation of the SIMPLE algorithm originally proposed by Caretto et al. (1973).

The discretization of the convective term in Equation (2.2) is handled by the HRIC scheme detailed in Section 2.1. Of particular note is that the default Courant number limits of 0.3 and 0.7, found in Equation (2.5), are replaced by the user adjustable parameters Cu_l and Cu_h with default values of 0.5 and 1, respectively. For steady free surface problems, where the

time step used is typically quite large relative to time varying problems, it is recommended by CD-Adapco to increase these limits to a value above the maximum Courant number expected within the domain in order to eliminate the use of the upwind scheme, and its associated smearing of the free surface. The effects of increasing these parameters are reported by Krasilnikov (2014) to have a favorable influence on the simulation results and are reported on in further detail in Chapter 4.

It is worth noting that, according to Thomas et al. (1992), with the VOF method, mass and momentum are conserved but the conservation of energy is not inherently guaranteed in the immediate vicinity of the free surface. Thomas et al. is addressing the method of Hirt and Nichols (1981), who only solve the equations of motion for the liquid phase, and mainly with applications on a staggered grid, where pressure and velocity points are not co-located. It is unclear whether these comments are relevant for the approach of Muzaferija and Peric (1999), who solve the equations of motion for both phases, and the Star-CCM+ solver which uses a co-located grid.

3.4 Discretization Schemes

Star-CCM+ offers a number of discretization schemes for both the temporal and spatial parts of the governing flow equations, some of which are only available in conjunction with specific models. For temporal discretization, first and second order schemes are available in steady and implicit unsteady forms. Explicit temporal schemes are only available for a limited subset of flow modelling schemes, such as the laminar coupled energy model. First and second order upwind schemes are available for spatial discretization, with additional options such as central differencing and bounded central differencing schemes being limited some to some particular models, such as large eddy simulations (LES).

For temporal discretization in the work presented here, the first order unsteady implicit scheme is used throughout. Even though the NACA 0012 case is expected to be fully steady, the NACA 0024 and KCS cases both feature some amount of separation and/or instability in the wake region, recommending the unsteady approach, and so the same approach was used with the steady NACA 0012 case in the interests of limiting sources of uncertainty when comparing the influence of various parameters on the results across the cases under investigation. In the preliminary KCS work, the second order option for time was investigated, but was found to increase computational demands for negligible improvement in accuracy or convergence of the simulation results, which is not surprising as the regions of unsteady flow are small and fairly weak in nature. The implicit aspect of the scheme, aside from being the only option available for the VOF model, offers enhanced stability which is of particular importance during the impulsive start-up approach used in the work and also permits Courant numbers greater than one. As the time history of the development of the flow is not of interest for the cases investigated here, there are no obvious drawbacks to the implicit approach. The number of inner iterations for the implicit scheme was left at the Star-CCM+ default of 5.

The spatial discretization selected was the default second order upwind scheme. The benefits of second order schemes for spatial discretization are well noted and the lower order option was not investigated in this work; the increased demands of the second order scheme were expected to be well worth any additional computational demands.

The solver for the segregated flow model used uses the algebraic multigrid method. There are a number cycles available for the multigrid solver, these were left at the Star-CCM+ defaults.

3.4.1 VOF Wave Damping

The VOF model in Star-CCM+ offers a function which dampens free surface waves in the vicinity of the domain boundaries. This is useful for preventing reflections from the boundaries interfering with the simulation results, without having to resort to employing a very large computational domain. The method implemented is that of Choi and Yoon (2009), where the velocity equations of the chosen discretization scheme are modified with a resistance term which is added to the velocity component normal to the free surface (typically the w component). This resistance term is features an exponential decay as it moves away from the boundary, becoming zero (no additional damping) at the user defined damping length way from the boundary.

3.5 Initial conditions

For the simulations undertaken in this work, the pressure within the domain is initialized to the hydrostatic pressure and the velocity is initialized to the inlet velocity. This impulsive type of simulation start does generate some severe pressure peaks and troughs around the body during the initial time steps, but with the implicit temporal discretization scheme, simulation stability during this startup phase was never an issue. A larger issue is perhaps the effect of these pressure pulses on the free surface, where their essentially impulsive nature sets up a fairly broad spectrum set of waves propagating through the domain. Those waves moving in the free stream direction are quickly flushed out of the domain, while those moving against the free steam may, depending on their group velocity, take quite some time to be flushed out of the computational domain or decay. Given sufficient amplitude, these waves may also reflect off the inlet boundary if there is no damping function applied to the free surface on this boundary in these simulations.

3.6 Post-processing

The Star-CCM+ software package includes an extensive collection of postprocessing tools to analyze and visualize simulation results with. These include point and line probes, cutting planes, 2D line plots, 2D vector plots, and 3D scalar plots. Reference data can be imported in tabular form to facilitate comparisons with other simulations or reference data, such as experiments.

It is possible to create user defined variables and field functions. For example, the equation for the drag coefficient (defined as per Equation (3.1)), was defined for each of the cases discussed in the ensuing chapters (using relevant characteristic areas and velocities). Star-CCM+ then allows the value of this coefficient to be monitored and recorded at each time step, permitting the user to assess the convergence of the drag coefficient throughout

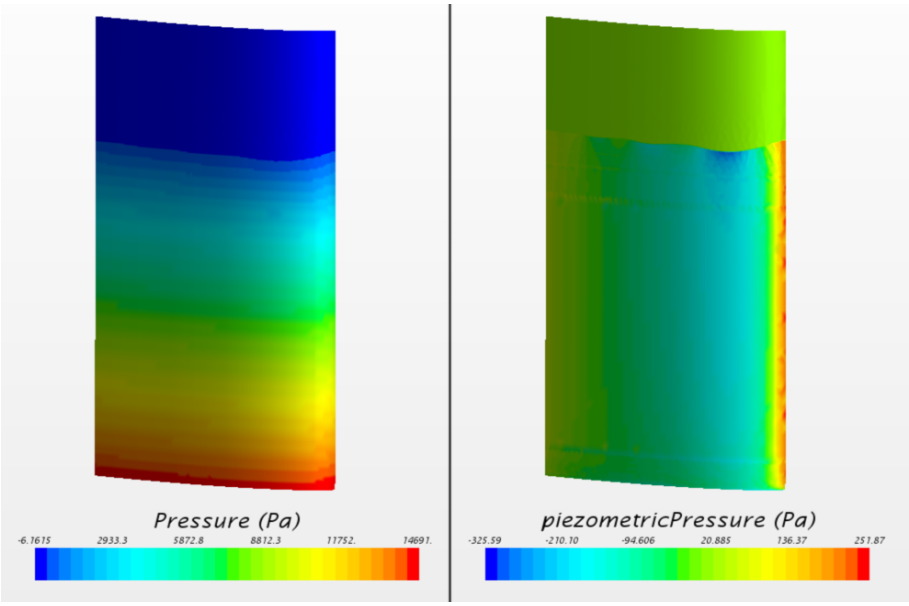

Figure 3.3: Pressures on the foil surface: standard pressure field (Left) and piezometric pressure field (Right)

the simulation (see Figure 2.1) without needing to save the entire flow field at every time step.

$$C_D = \frac{F_D}{\frac{1}{2}\rho V^2 S_w} \tag{3.1}$$

The ability to define custom field functions is quite useful: for free surface flows there is a tendency for the hydrostatic pressure gradient to dominate a normal color or contour plot and hide the influence of the flow field on the body surface pressures. By creating a custom pressure field which defines the piezometric pressure, essentially the pressure field minus the hydrostatic pressure of the undisturbed free surface, the influence of the flow field on the body pressures are much more readily visualized as in Figure 3.3. Further details for this custom field function can be found in Appendix A.

The two dimensional plotting ability of Star-CCM+ is a very powerful and feature rich tool. However, some of these features must be used with some care, the smoothing function in particular. In general, smoothing of data, such as a planar intersection with the free surface for example, makes it easier to interpret the discrete data generated by CFD with respect to the continuum that is being modelled. However, the spline function that is used to smooth the 2D data can in some circumstances provide a misleading interpretation, such as in Figure 3.4, where the smoothed data suggests that the small amplitude waves extend right up to the inlet boundary, while the unsmoothed data shows that this is clearly not the case.

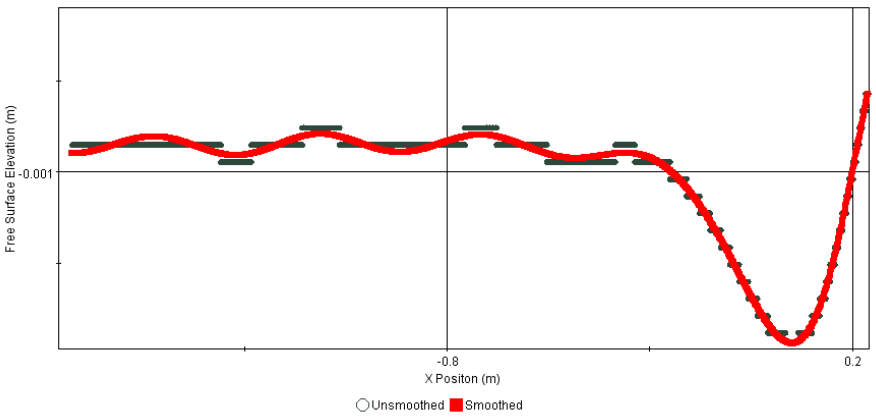

Figure 3.4: Potentially misleading effect of smoothing function on 2D data representation of free surface elevation

Chapter 4

2D NACA 0012 Foil

In order to explore the influence of mesh and time step resolution on the free surface in a simpler and less computationally demanding manner, the classic two dimensional case of a fully submerged NACA 0012 foil with free surface was investigated, as per the experimental setup used and reported by Duncan (1982). This case offers a fairly simple free surface flow where the complexities of a surface piercing body are conveniently circumvented. The results presented in the Duncan paper cover a range of angles of attack, mean free stream velocities, and foil submergences, all of which influence the size and nature of the resulting wave system, with the waves being steep enough to break in some cases.

The foil chord is $20.3\,cm$. For this work, the case with the deepest immersion of $26.1\,cm$ at a 5° angle of attack and $80\,cm/s$ mean free stream velocity was selected as the benchmark case, with the objective being to avoid any complications in modelling the free surface arising from very steep or breaking waves. The simulations with the 2D NACA 0012 foil were completed with Star-CCM+ version 8.06.007.

4.1 Problem Setup

As the VOF Waves feature of Star-CCM+,which makes the setup of a two phase free surface flow problem substantially easier, is not available for pure 2D meshes, this problem was investigated as a quasi 2D simulation with the width of the domain kept small and the side boundaries configured as symmetry planes. The upper and lower boundaries were modelled as slip walls with the inlet and outlet boundaries modelled as fixed velocity and hydrostatic pressure, respectively. The distance from the undisturbed free surface to the foil is $26.1\,cm$ and the distance from the foil to the lower domain boundary is $17\,cm$, in accordance with the configuration used in the experiments.

The reference frame was set as shown in figure 4.1, with the origin centered laterally at the undisturbed free surface and directly above the 50% chord point of the foil, the x-axis aligned with the free stream flow direction, and the y-axis pointing vertically upwards. As the problem is analyzed as a 2D problem, the z-axis is essentially ignored and all results are extracted from the middle of the domain ($z = 0$ plane). The inlet and outlet boundaries are located 8.5 chord lengths upstream and 16.5 chord lengths downstream of the origin, respectively.

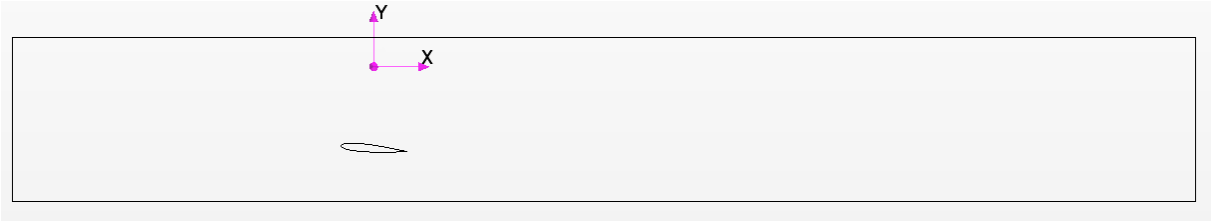

Figure 4.1: NACA 0012 reference frame

In order to reduce the wave amplitude, and thus the gradients, at the outlet, the VOF damping option is enabled on this boundary with a damping length of 1.25 m. The majority of solver parameters were left at their default settings, as discussed in Chapter 3, with the only time step and Courant number limits being changed, as discussed in the ensuing sections.

The simulation time required for convergence of the solution was found to be 17 s for the initial cases, and proved to be adequate for all of the simulations undertaken with the NACA 0012 foil.

4.1.1 Meshing

As with the rest of the work undertaken in this thesis, the mesh type used is of a trimmed hexahedral type, with prism cells near the surface of the foil in order to resolve the boundary layer. The prism mesh consists of 5 layers and is configured such that wall functions are used, with a target y^+ of 50 and the resulting wall distance calculated according to Equation (2.9).

The mesh features a fairly coarse base element size in order to reduce the cell count in the far field, with local refinements around the free surface and foil. Refinements around the free surface are anisotropic in nature to enable independent control of the refinement in the X and Y directions, and thus investigation of the number of cells per wave length (X direction), per wave amplitude (Y direction), and mesh aspect ratio in the vicinity of the free surface. The mesh refinement block around the foil is isotropic in nature and limited to the region near the foil; as the primary focus of this case is on the free surface, optimal resolution of the far field wake of the foil was deemed unnecessary. The free surface refinements in both the X and Y directions extend throughout the domain. This is due to concerns that having jumps in refinement around the free surface, at least in the direction normal to the undisturbed free surface (Y direction, in this case), can cause some instability in the simulation, but mainly due to a desire to ensure that mesh parameters which may influence the numerical aspects of the solution process (cell aspect ratio, number of cells per wavelength/height) are consistent throughout the domain.

It should be noted that the mesh thickness is greater than one cell (Figure 4.2). This is due to reports that the solution can converge more rapidly in the quasi 2D case with several cells thickness between the bounding symmetry planes.

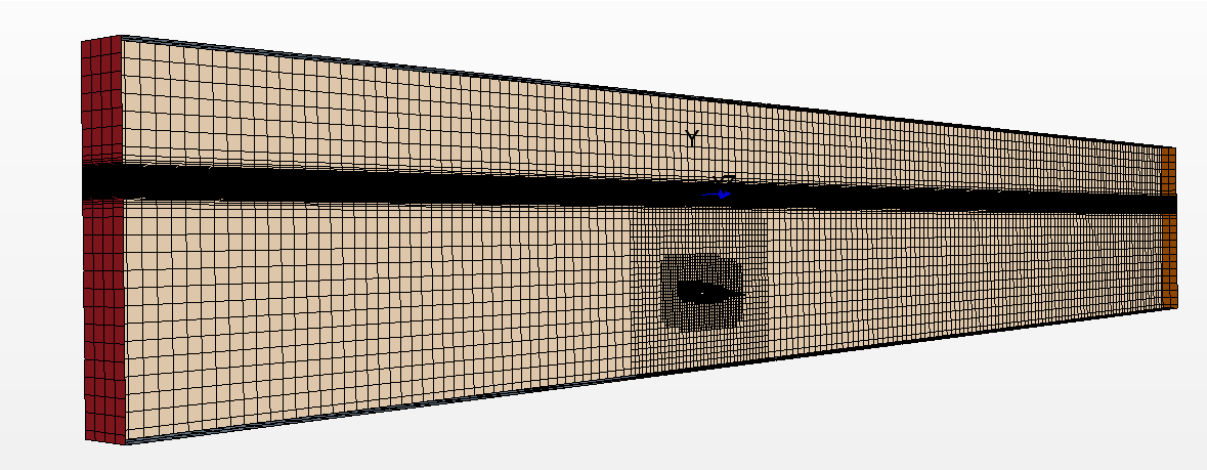

Figure 4.2: NACA 0012 mesh

4.2 Courant Number Limit Investigation

A comparison of using the default Courant number limits and also significantly increased Courant number limits (thus enforcing the HRIC scheme over the entire free surface) was undertaken at time steps of 0.01 s, 0.005 s, and 0.0025 s, with a basic mesh based on the ITTC mesh guidelines discussed in Section 2.2; 40 cells per wavelength and 10 cells per wave amplitude. From the experimental data the wavelength and wave amplitude were expected to be 41.8 cm and 1.6 cm, respectively, leading to a cell size of 1.05 cm in X and 0.08 cm in Y in order to obtain the desired resolution. Due to the aforementioned refinement limitations of the trimmer mesh, the actual cell size obtained was 0.75 cm in X and 0.047 cm in Y, resulting in 58 cells per wavelength and 17 points per wave amplitude. The foil refinement block was set to 2.5% of the foil chord length (5 mm). Total cell count for this mesh was 269779.

At the coarsest time step, where the Courant number around the free surface ranged from 0.6 to 3.6 (above the default lower Co limit of 0.5), there is significant smearing of the free surface and the waves decay quickly (fig. 4.3). Increasing the Courant number limits to 10 (low) and 20 (high) substantially reduces the damping of the waves due to diffusion, as shown in Figure 4.4, and keeps the interface sharp (to within $1-3$ cells as per Ferziger and Perić (2002)). The difference between the default and high Courant number limit results reduces with decreasing time step; by 0.0025 s, there is a negligible difference. This is as one would expect, with the 0.0025 s time step resulting in Courant numbers at the free surface of 0.15 to 0.9, which places a good part of the free surface in the HRIC range (Co below 0.5) and the rest in the blended range (Co between 0.5 and 1.0).

One particularly unusual result was noted at the 0.005 s time step, with default Courant number limits; the free surface actually displayed negative damping behaviour with steadily increasing wave amplitude in the downstream direction (see Figure 4.5), until the damping function applied to the outlet boundary becomes dominant. Indeed, this particular configuration appears to be right on the edge of numerical stability as it actually crashed the first time it was attempted to run, but successfully reached the set simulation time on the second attempt.

Based on the above results, the high Courant number limits were used for the remainder of the results discussed in this, and ensuing, chapters.

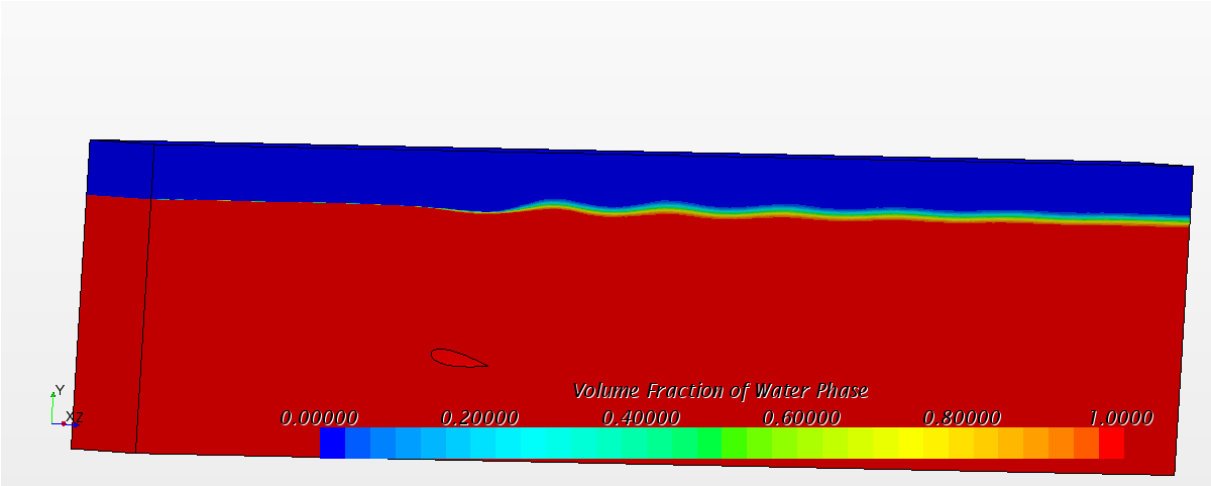

Figure 4.3: Diffusion of the free surface with default Co number limits and high local Courant number

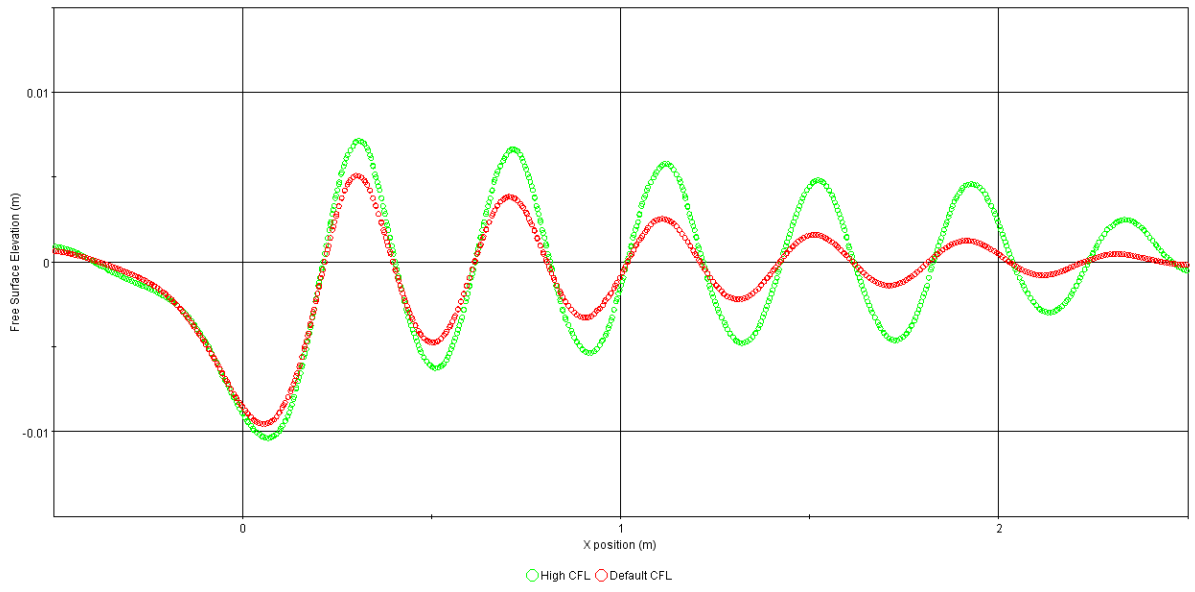

Figure 4.4: Heavily damped free surface wave elevations, with default Co limits, due to smearing of free surface, compared with a similar case with higher Co limits and a sharper interface

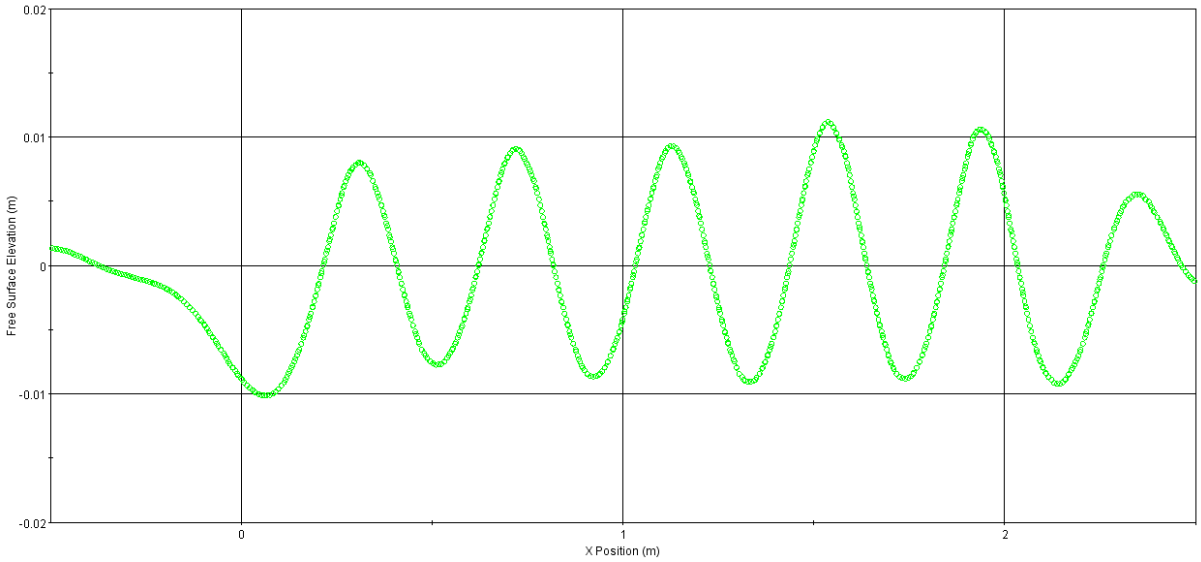

Figure 4.5: Free surface profile featuring negative damping with default Co limits and a time step of 0.005 s.

4.3 Spatial and Temporal Resolution

In addition to the various time steps mentioned in the previous section, the spatial resolution was also investigated. Rather than a conventional mesh convergence study, where the mesh resolution is increased, but the mesh topology and cell aspect ratio are kept constant, this study varied the number of cells per wavelength and per wave amplitude in the free surface region independently, with the result being that a variety of cell aspect ratios were also tested. The effects of spatial resolution were first investigated with a time step of 0.005s, as there was, with the high Courant number limits, no difference observed to the 0.0025s time step results. This time step of 0.005s is at the high end of the range given by the ITTC in Equation (2.8) (0.00264s - 0.00528s), but is higher than the 0.0038s step for a 58 cell per wavelength mesh given by Equation (2.7) from CD-Adapco. With these mesh resolution tests it was noted that the free surface profile fell into either the "damped" or "undamped" category as shown in Figure 4.6, with the transition being very abrupt below a threshold value for a given parameter; the mesh resolution parameters capable of triggering this behaviour were found to be less than 7 cells per wave amplitude, or a cell aspect ratio greater than 8. The sensitivity to aspect ratio was found to be independent of overall resolution, with meshes of similar aspect ratios but up to three times the resolution displaying the same results. It was not possible, given the wavelength and amplitude in these tests, to generate a mesh within the aforementioned limits with fewer than 58 cells per wavelength, which was found to be adequate resolution for the time step of 0.005s.

With the basic requirements for spatial resolution established, a more formal time step investigation was carried out with a mesh featuring 9 cells per wave amplitude, 58 cells per wavelength, and a cell aspect ratio of 8. Total mesh size was 167967 cells. Instead of a gradual change in free surface profile with time step as found with the default Courant number limits, a fairly abrupt step change in the free surface profile was noted, with the the results across this step being identical to the mesh refinement investigation. After further investigation, this abrupt change was found occur between time steps of 0.00575 s and 0.006 s, as

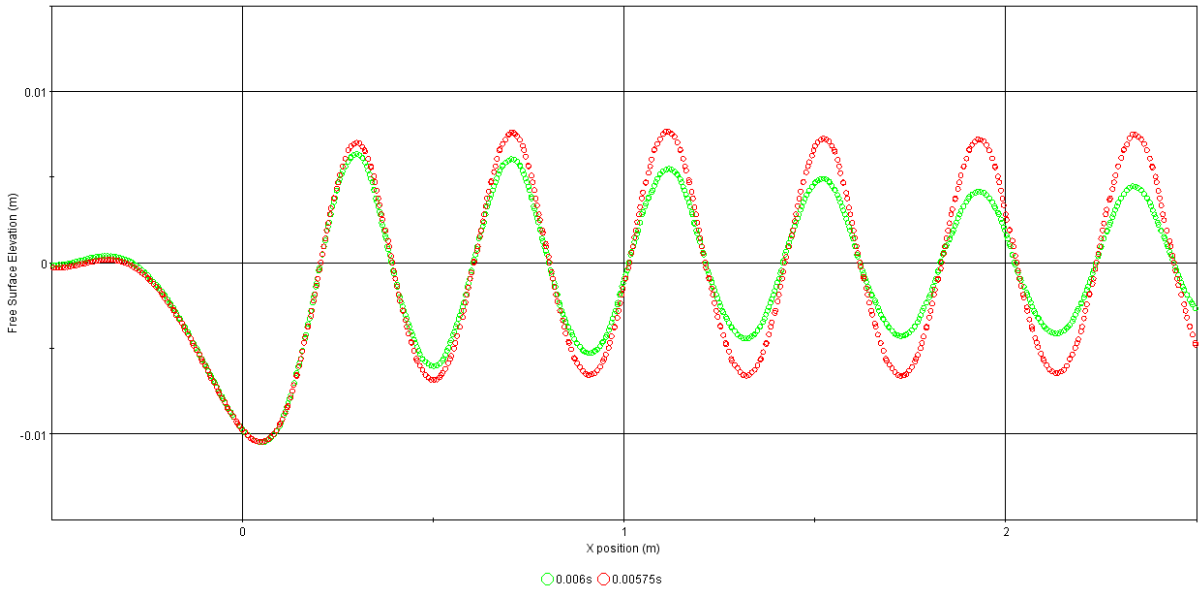

Figure 4.6: Abrupt change in free surface profile with a change in time step from 0.00575 *s* to 0.006 *s*

shown in Figure 4.6.

The flow problem represented by this 2D NACA 0012 foil configuration is a steady state one, so it remains of great interest to try and find a numerical solution that is not dependent on time step. In general there is some interplay or possibility to trade off between spatial and temporal resolution, in a time invariant problem at least, and the results of the time step investigation suggest that there is indeed a critical resolution threshold. The CD-Adapco recommendations, with 80 cells per wavelength and 20 cells per wave amplitude, were used as a starting point for creating a mesh of sufficient resolution to yield a time step independent solution. The resulting mesh featured 85 cells per wavelength and 17 cells per wave amplitude, due to the aforementioned quantisation limitations of the Trimmer mesher, while the remainder of the mesh within the solution domain remained unchanged from previous cases. The cell aspect ratio was 8 and total mesh count was 258807 cells. An initial time step of 0.005 *s* was used, as previous results indicated that a finer time step was not needed to create a baseline result for this particular investigation, especially considering the increased mesh resolution around the free surface. Progressively coarser time steps were run, all the way up to 0.05 *s*, with negligible difference in the free surface profile observed (excluding the region downstream from x=2.1 *m*, which was influenced by the VOF damping function), at which point it was concluded that a time step independent solution had been found. The wave profiles for the 0.05s and 0.005s cases are compared in Figure 4.7.

4.4 Comparison with Experiments

The results of the numerical simulation for the time step independent mesh of 258807 cells, with a time step of 0.005 *s* was selected as the case to compare against the experimental results of Duncan (1982). Notably, any of the so called "undamped" results obtained in this section could be used for the comparison as the variation in wave profile between these re-

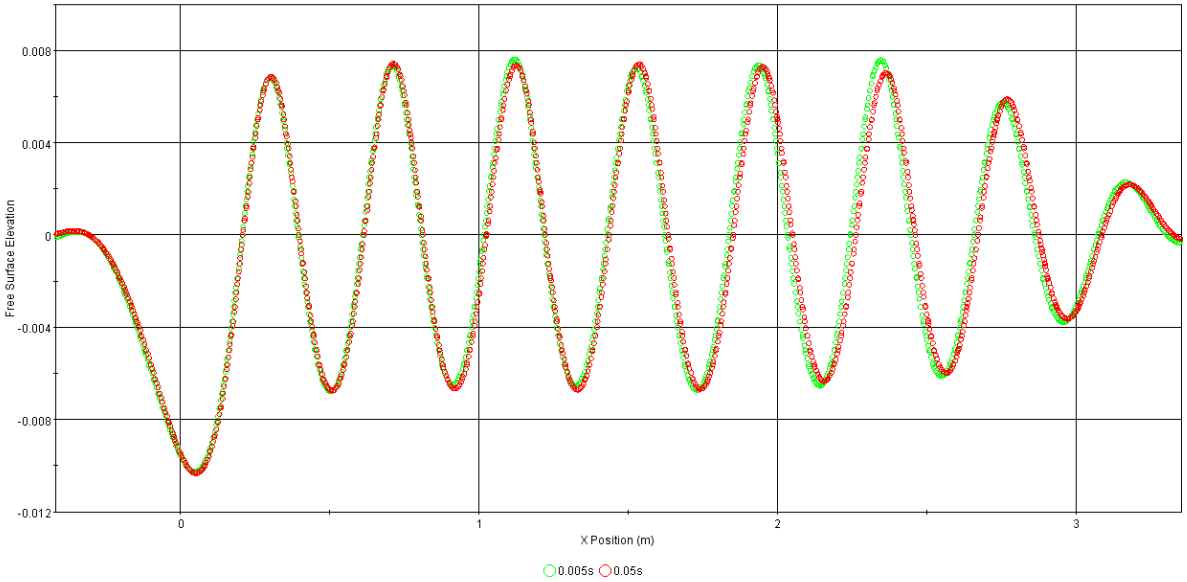

Figure 4.7: Comparison of free surface elevation for 0.005s and 0.05s time step solutions, with a cell count of 258807, showing time step independence

sults is on the order of $1-2\%$ in the worst case. The experimental and numerical results are compared in Figure 4.8. It can be observed that both the wave amplitude and wave length are lower than the experimental values, and the first wave trough in particular is underpredicted.

It should be noted that, while the experimental results claim an accuracy of $\pm 0.3\,cm$ (or about 19% of the maximum wave height), the wave profile is not presented in tabular form and thus the experimental data presented in Figure 4.8 is a digitized copy of the plots presented in the original paper. As such, the total uncertainty of the experimental data presented here is almost certainly higher than the claimed value of $\pm 0.3\,cm$.

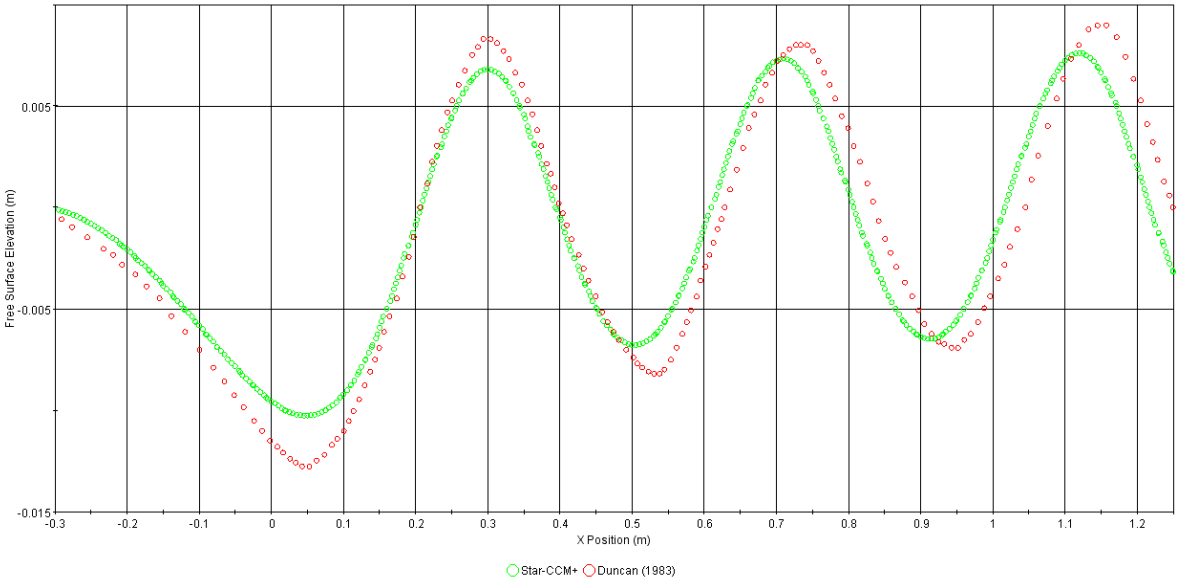

Figure 4.8: Comparison of numerical solution, for the time step independent mesh of 258807 cells, with a time step of 0.005 s, and experimental free surface profiles

4.5 Outlet Damping

As mentioned in Section 4.1, a damping function was used on the outlet boundary to limit gradients at the outlet boundary and minimize risk of waves reflecting back into the domain. While the damping length was set to 1.25 m , there was some concern about how far upstream the effects of this damping function might be felt. Thus, the computational domain was extended by 2.5 m downstream using a mesh extrusion operation. The mesh topology and damping length were kept identical to the the original domain. The results for the original and extended domain are compared over the length of the original domain in Figure 4.9, where it can be observed that there is some noticeable reduction in wave amplitude one to two wavelength upstream of where the damping function terminates.

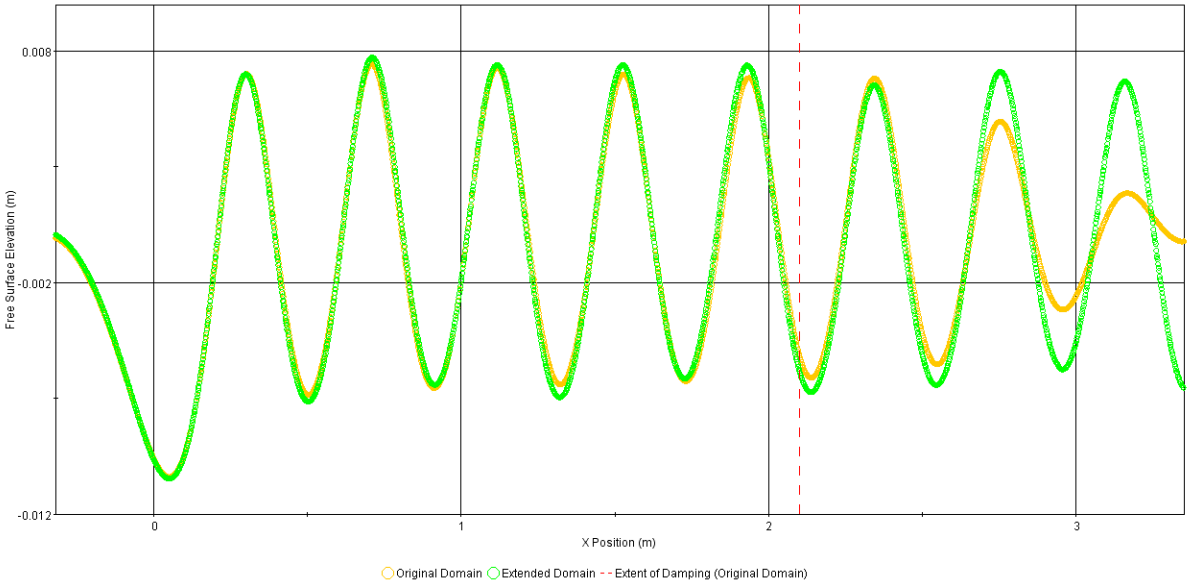

Figure 4.9: Comparison of original and extended domains showing the influence of outlet damping function on free surface $1-2$ wavelengths upstream of the damping length

4.6 Residual Convergence

The residual convergence for the NACA 0012 simulations are generally acceptable, in contrast to the KCS example given in Figure 1.2, but the desired $3-4$ orders of magnitude reduction was not achieved in any of the simulations. An example is shown in Figure 4.10, for the 258807 cell mesh at a time step of $0.005\,s$. The air residual is noteworthy for displaying more or less negligible convergence. The reasons and significance behind this are unclear. It was suspected that there was not enough distance between the free surface and the upper domain boundary, but increasing this distance had no effect on the residual convergence.

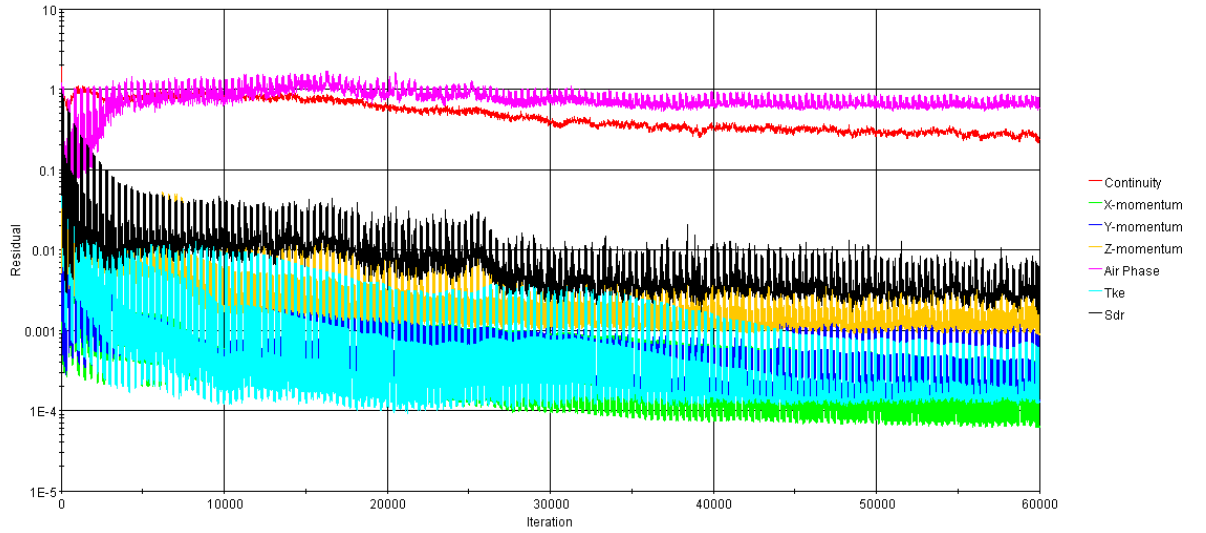

Figure 4.10: Residual convergence for the 258807 cell mesh at a time step of 0.005 *s*

4.7 Discussion

The investigation of the surface piercing NACA 0012 foil has provided some valuable insights into the behaviour of the Star-CCM+ software package when it comes to modelling of free surface flows. The importance of increasing the default Courant number limits, the critical limits of resolution, both temporal and spatial, and cell aspect ratio for optimal results of the free surface are perhaps the most important findings. For a mesh meeting the minimum resolution requirements, the Cd-Adapco time step recommendations (eq. (2.7)) give quite a conservative value, while the coarse end of the range recommended by the ITTC (eq. (2.8)) appears to be adequate in the cases investigated here. The possibility of creating a mesh of sufficient resolution to obtain a time step independent solution is an interesting one. Given that, for the meshes tested, time steps from both equations 2.7 and 2.8 provided comparable results to the time step independent solution, it becomes an interesting question of whether or not opting for a mesh of adequate accuracy for time step independence is computationally more efficient or not. In this quasi 2D application, the answer is quite clear; a gain of approximately 50% in spatial resolution for a reduction in temporal resolution by a factor of 10 means that the time step independent mesh is the fastest approach. It remains to be seen whether a time step independent solution can generally be found for a time invariant 3D problem, and if so whether it remains computationally more efficient as it is in the 2D case.

Within the time step investigation, the nature of the abrupt step change, occurring over a in time step delta of only 0.00025 *s* (it is expected that further investigation could reduce this range even further), is unusual and suggests some sort of conditional statement governing the underlying numerics being triggered. However, there is no discussion of such a condition within the Star-CCM+ documentation. This is the only notable numerical issue found during these tests as the marginal stability of the 0.005 *s* time step case was rectified through the use of increased Courant number limits.

The agreement obtained with experimental results is not particularly strong, with both the wave amplitude and wave length being underpredicted numerically. The underprediction

of the first wave trough, and to a lesser degree the successive wave amplitudes, seems to be a common issue with RANS based solutions of this problem, based on results reports by Ferziger and Perić (2002); Löhner (2008); Ali and Karim (2010); Muscari and Mascio (2003). The discrepancy in wave length is of greater concern, as the relationship between wave length and propagation speed is well defined, and correctly capturing the zero crossing period of a wave is typically easier and more accurate than capturing the amplitude of the same wave. Unfortunately, no uncertainty estimate is given for the velocity in the Duncan (1982) results. Other than a discrepancy in velocity, it is hard to identify where other shortcomings in the modelling approach may be found; the tank depth is approximately the same as the wave length, so shallow water effects should not be a concern, leaving the quasi 2D approach (as opposed to a proper, rigorous 2D approach) as the primary suspected culprit. The large uncertainty in the experimental results also makes it difficult to be assess the accuracy of the numerical results. In retrospect it may have been wiser to run a shallower submergence case to have a larger amplitude, non-breaking wave in order to limit the error margin imposed by the experimental accuracy and digization of the reported results. Ultimately, however, it has been the variation of parameters within the numerical simulations, and the comparison of these results, that has provided the most significant benefits and insights.

Chapter 5

NACA0024 Surface Piercing Foil

Following on from the findings obtained in Chapter 4, the three dimensional case of the surface piercing NACA 0024 foil has been investigated and compared with the experimental data published by Metcalf et al. (2006), which includes an extensive data set available for download from the University of Iowa (2013). The experimental data includes free surface elevations over a substantial region around the foil, as well as an extensive set of pressure measurements on the foil surface. An integral value for drag on the foil is, unfortunately, not included in the data set.

The simulations with the surface piercing NACA 0024 foil were completed with Star-CCM+ version 9.02.007. In order to verify consistency across software versions, one case was run with Star-CCM+ version 8.06.007, which yielded identical results to those from version 9.02.007.

5.1 Problem Setup

The computational domain was configured to match the sectional dimensions of the towing tank at the University of Iowa, where the experiments were conducted. A symmetry condition was applied at the foil centerline for the simulations (unless otherwise noted). The half domain breadth is 1.525 m, water depth is 3.05 m, and foil immersion is 1.5 m. The upper, lower, and side walls were modelled as slip walls. While this neglects any influence of viscous effects on interaction effects such as blockage, this does offer the possibility of capturing, with fairly good accuracy, any pressure interaction between the foil and the domain boundaries, as in the actual experiments. The upstream boundary is a velocity inlet, placed 2 chord lengths upstream, and the downstream boundary is a pressure outlet, placed 5 chord lengths downstream, set to the hydrostatic pressure. As with the NACA 0012 case, the simulation is started impulsively, with pressure set to the hydrostatic pressure of the undisturbed free surface, and initial velocity set to the inlet velocity.

The reference frame is centered at the intersection of the leading edge of the foil and the undisturbed free surface, with the x-axis in the direction of the free stream velocity, the z-axis pointing vertically upwards, and the y-axis oriented to give a right handed reference frame, as shown in figure 5.1. The inversion of the X and Y axes, with respect to conventional reference frames used in seakeeping problems, is to keep the reference system consistent with that used in the experimental data.

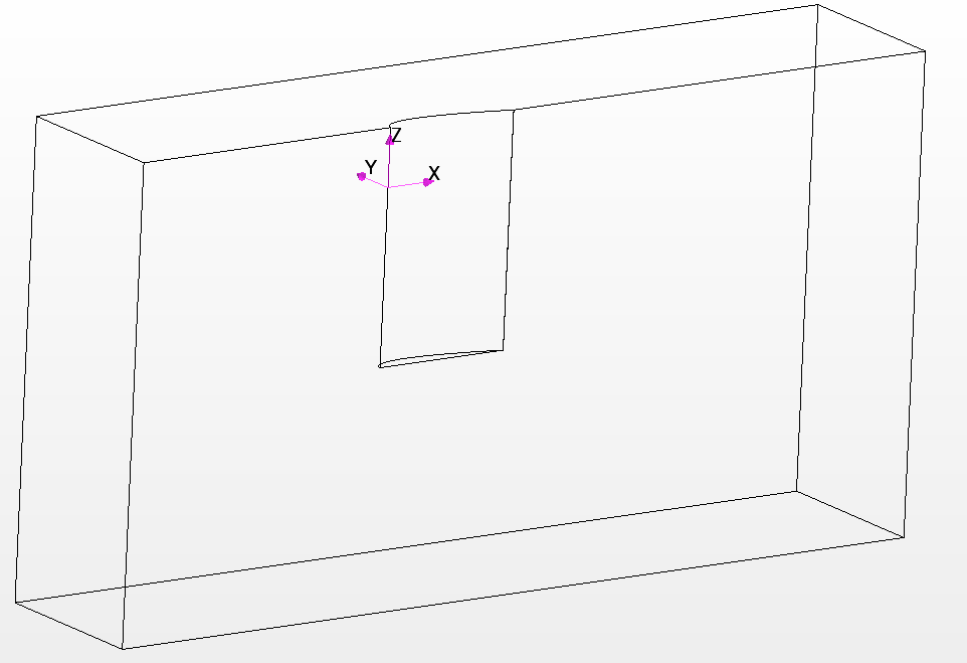

Figure 5.1: Surface piercing NACA 0024 domain and reference frame

Based on the results from Chapter 4, the Courant number limits were increased for all of the simulations with the NACA 0024 foil, with the lower and upper limits set to 20 and 30, respectively. The simulation time required for convergence of the solution was found to be $27\,s$ for the initial cases, and proved to be adequate for all of the simulations undertaken with the NACA 0024 foil, with the only notable variation being slightly larger and more erratic variations in the convergence of the force coefficients for the coarser time steps and meshes.

5.1.1 Meshing

As in the previous case, the mesh is of a trimmed hexahedral type, with prism cells near the surface of the foil in order to resolve the boundary layer. The mesh features a fairly coarse base element size in order to reduce cell count in the far field, with local refinements around the free surface and foil. The foil refinement block is limited to the region near the foil: as the primary focus of this case is on the free surface, optimal resolution of the foil wake is not a priority.

The free surface region includes a refinement normal to the undisturbed free surface (Z direction) which extends throughout the domain with a thickness that is 10% greater than the maximum wave amplitude of $4\,cm$ reported in the experimental data. This, as discussed previously, is due to concerns about the propagation of waves from the impulsive start and the possibly adverse effects a jump in refinement normal the free surface could have on the quality of the results. However, this approach does, for this case at least, lead to extremely high costs in terms of mesh size. Refinements parallel to the undisturbed free surface are made through the use of wedge shaped blocks in order to minimize the mesh cell count. Initial attempts used a refinement extending throughout the domain, as in the 2D case, but this proved to be unfeasible due to the resulting mesh size. The wedges use refinement levels

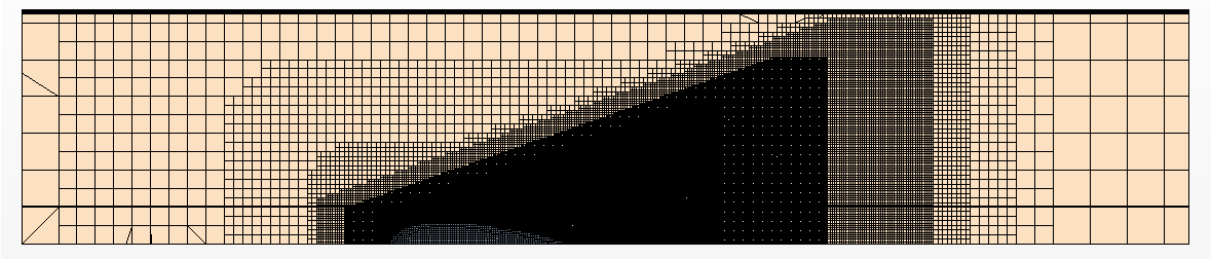

Figure 5.2: NACA 0024 free surface mesh refinement blocks

that are tapered in a series of five to six blocks (see Figure 5.2), starting from 0.5 chord length upstream to 3 chord lengths downstream of the foil, in order to ensure a smooth transiting from the fine region near the foil to the coarse far field mesh.

Determining the characteristic wavelength for the 3D case, with a diverging as well as transverse wave system, is more complicated than in the 2D NACA 0012 case. Due the the fine trailing edge of the NACA 0024 profile, there is only one wave system (bow wave). In the general ship case, there will be both bow and stern diverging wave systems, which will interact with each other, creating a potentially very complicated free surface profile. In order to develop a working method that will remain manageable in the face of an unknown free surface pattern, the transverse wavelength was selected for use as the characteristic length. In this case, from the experimental data, the transverse wavelength was found to be $0.26\,m$. If this information is not known beforehand, it can be estimated with good accuracy by Equation (5.1), found in Faltinsen (2005), where λ is the wavelength.

$$\lambda = 2\pi Fr^2 L \tag{5.1}$$

In spite of the efforts to minimize the volume of the mesh refinement blocks, generating an initial mesh based on the CD-Adapco recommendations utilizing 80 cells per wavelength and 20 per wave amplitude proved incredibly costly in this case, resulting in a mesh of 8.71 million cells for the half domain, with over 70% of these in the free surface refinement region. This is primarily a result of the wave system generated by such a bluff body like the NACA 0024 foil, which is characterized by a large amplitude and steep (short) wave for the relatively low Froude number of 0.19, compared to normal ship like forms. However, the situation was not helped by selecting a mesh base size based solely on the desired Z direction resolution; the resulting quantization of the mesh cell size in the X and Y directions led to a mesh with 120 cells per wavelength instead of the target 80, and an aspect ratio of 2. The difference in refinement between the extremely fine free surface region and the coarser foil refinement block also required a fairly large amount of manipulation of the prism layer settings in order to arrive at an acceptable compromise in terms of cell size progression between the prism layer and outer volume mesh. The result, shown in Figure 5.3, is a prism mesh of higher thickness than usual consisting of 8 layers and a stretching ratio of 1.18.

5.2 Mesh Resolution Study

Initial efforts to run this mesh at the time step calculated from Equation (2.7) of $0.001\,s$ proved to be excessively time consuming for the available resources, even when attempt-

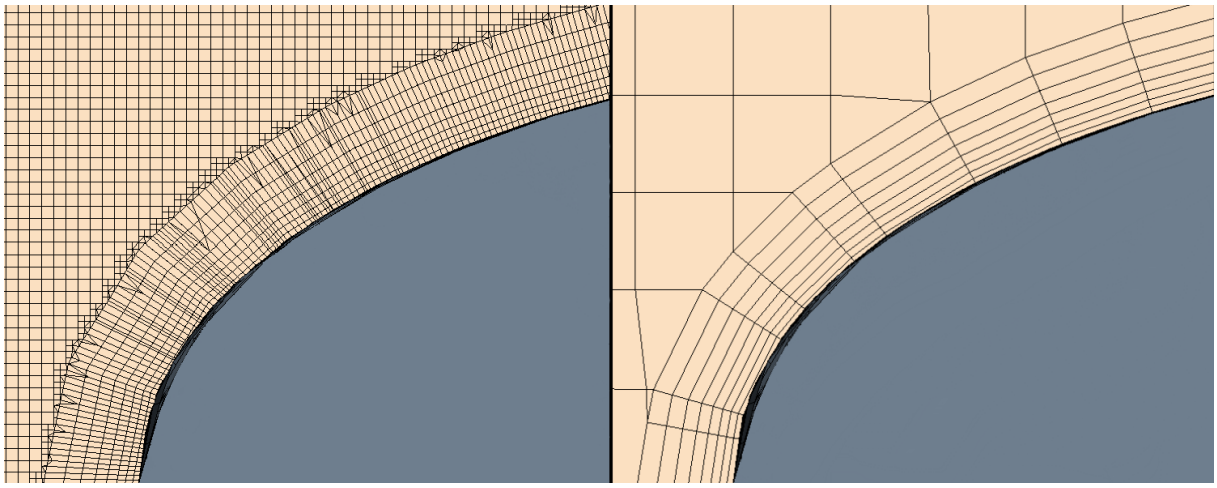

Figure 5.3: Prism layer to volume mesh interface in free surface region (Left) and away from free surface region (Right), showing the significant variation between the region influenced by the free surface refinements and that which is not

ing to utilize up to 120 cores. As a result, the simulation was run with a time step of 0.005 s since, based on the experiences from the NACA 0012 case, the mesh spatial resolution was expected to be adequate for obtaining a time step independent solution. Even after reducing the computational demands by a factor of five, the simulation took some 26 hours to complete on 60 cores.

Given the already high cell count of the initial mesh, the traditional mesh convergence investigation has actually been reversed here, and a series of coarser meshes than the original one investigated. The first coarsening step was achieved by removing the innermost wedge refinement block, which made a significant reduction in mesh size to 4.67 million cells. The remaining coarsening steps were achieved by increasing the base size of the mesh by powers of 2, resulting in meshes of 0.21, 0.52, 1.89 million cells, in addition to the two aforementioned meshes. The results of this study are shown in figures 5.4 and 5.5, which show the convergence of the total drag coefficient, and maximum and minimum wave elevations within the domain, respectively. It can be observed that the total drag coefficient is converged at the 4.67 million mesh, although the convergence is not smoothly monotonic due to the wiggle around 2 million cells. The free surface minimum elevation shows good convergence above 2 million cells, while the maximum elevation shows 12% fluctuation between 2 and 8.7 million cells. Given the bluff nature of the NACA 0024 foil and the steep gradients around the leading edge, where the maximum free surface elevation is found, it is to be expected that this region shows increased sensitivity to mesh resolution.

A mesh aspect ratio investigation was conducted with the 4.67 million cell mesh. Unfortunately, given the very high Z resolution, and the 60 cells per wavelength, of this mesh, the scope of this investigation was much more limited than in the NACA 0012 case; aspect ratios of 4 and 8 were investigated in addition to the original aspect ratio of 2. Efforts to investigate higher aspect ratios by increasing Z resolution further lead to meshes too large to fit in the 24 GB of system memory available, while with only 15 cells per wavelength at an aspect ratio of 8, reducing resolution further is not feasible either. Indeed, as can be seen in Figure 5.6, the results for aspect ratios of 2 and 4 show acceptable agreement while the aspect ratio 8 results show a complete inability to resolve the free surface profile. This is almost certainly

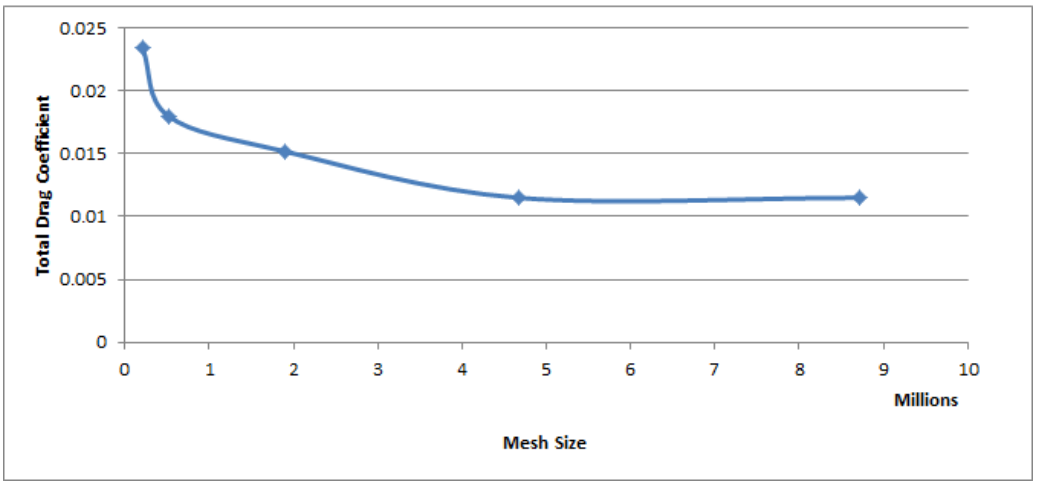

Figure 5.4: Convergence plot of total drag coefficient for the NACA 0024 surface piercing foil, at a time step of 0.005 *s*

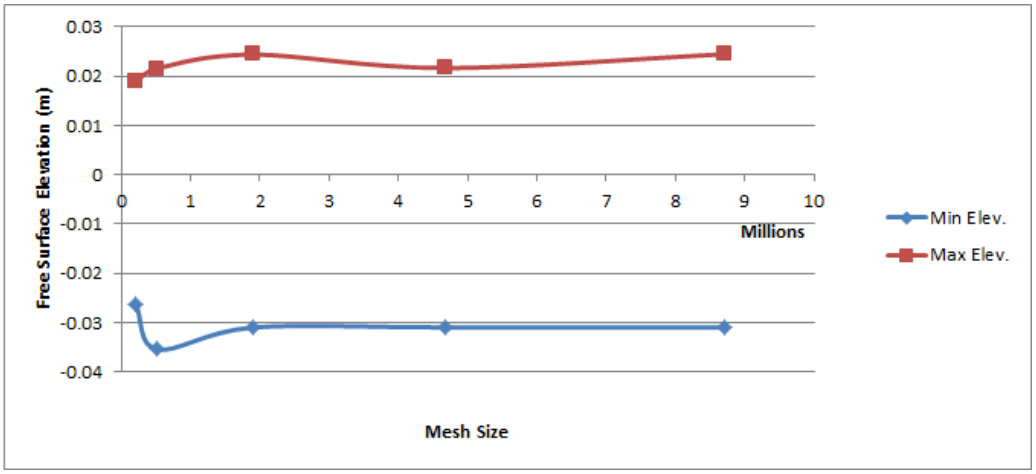

Figure 5.5: Convergence plot of maximum and minimum free surface elevation for NACA 0024 surface piercing foil, at a time step of 0.005 *s*

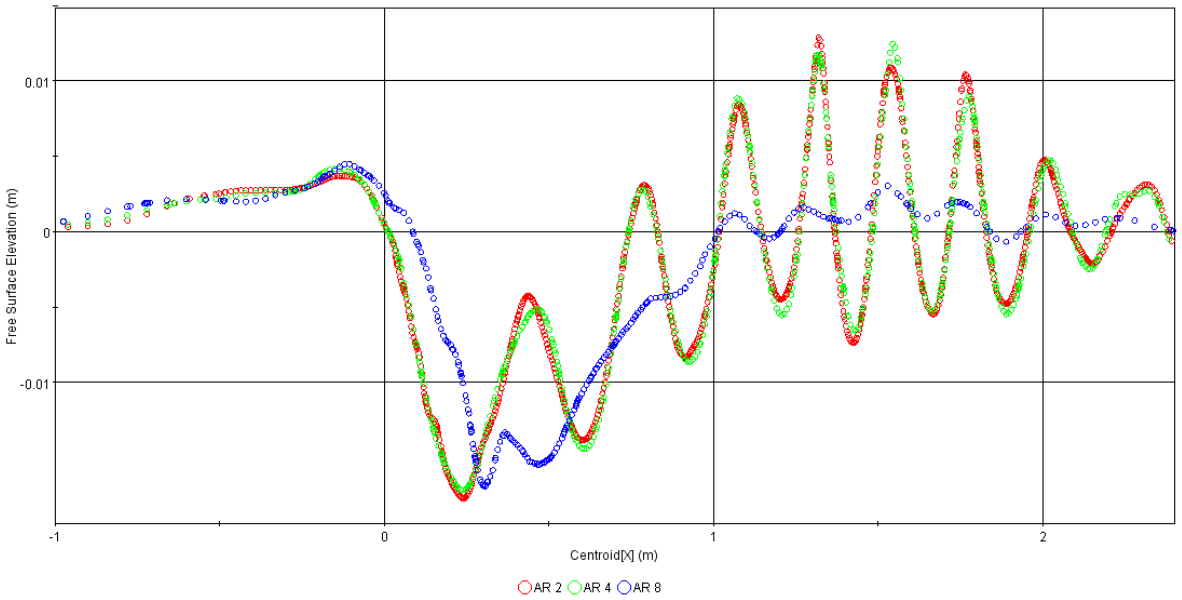

Figure 5.6: Effect of cell aspect ratios of 2, 4, and 8 on the free surface profile at Y=0.25 *m*

due to insufficient resolution rather than any issues with cell aspect ratio.

5.3 Time Step Investigation

A time step investigation was conducted based on the 4.67 million cell mesh, as this mesh was expected to be below the required threshold for time step independence. Time steps of 0.1, 0.05, and 0.001 seconds were investigated in addition to the 0.005 *s* time step from the mesh refinement study. The results for free surface extrema and total drag coefficient are presented in Figures 5.7 and 5.8, respectively. It can be observed that the free surface maximum and minimum elevations are independent of time step when a time step of 0.005 *s* or less is used, and the same holds true for the total drag coefficient. This time step is much coarser than the 0.0029 *s* obtained from Equation (2.7) and slightly coarser than the high end of the $0.00418 - 0.00209$ *s* range given by Equation (2.8).

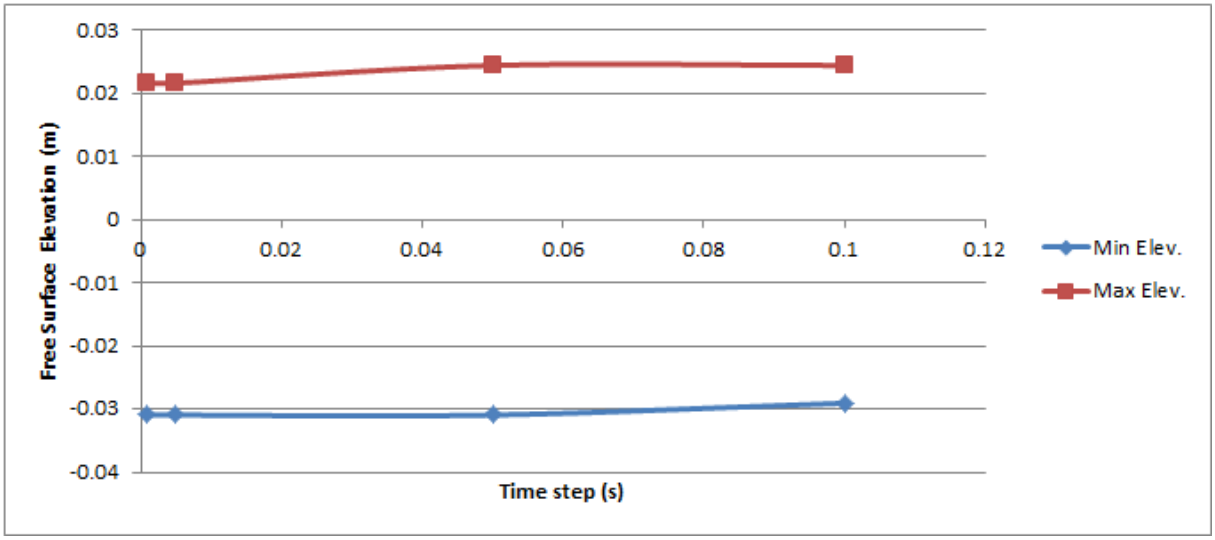

Figure 5.7: Time step dependency of free surface elevation extreme values for the NACA 0024 case, 4.67 million cell mesh

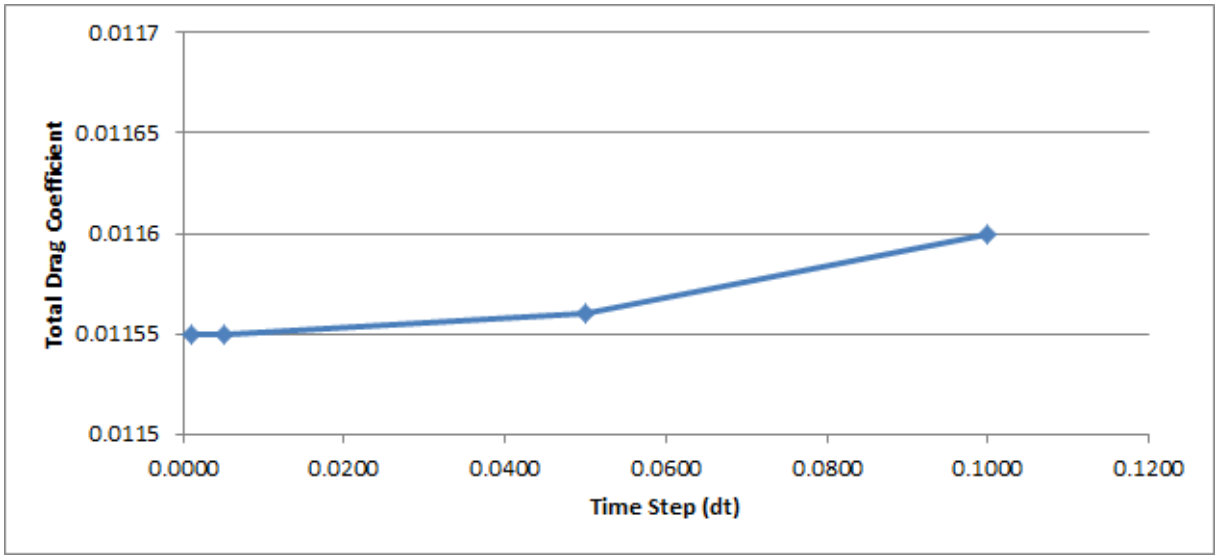

Figure 5.8: Time step dependency of total drag coefficient for the NACA 0024 case, 4.67 million cell mesh

5.3.1 Free Surface Elevation and Surface Pressure

The wave profiles at a longitudinal cut 0.25 m off the foil centerline are compared in Figure 5.9 for time steps of 0.1s, 0.005 s, and the reference experimental data. As in the KCS case, the free surface displayed a dependency on time step with the finer time step resulting in overprediction of the far field wave elevations, in comparison to the experimental data. There is a difference of approximately 2.5% in the pressure drag coefficient between the 0.005 s and 0.1 s time step results (frictional drag coefficients are within 0.1%), which is smaller than might be suggested by the differences in the far field wave profiles. However, the pressure on the foil surface for longitudinal cuts at $Z = -0.1728\,m$ and $Z = -1.11648\,m$ are presented in Figures 5.10 and 5.11, respectively, where it can be seen that the pressure between the 0.005 s and 0.1 s time steps are in very good agreement with each other and the experimental values as well. This agreement in pressure is in marked contrast to the free surface elevation on the foil (fig. 5.12), where the numerical results show smaller amplitudes and shorter wave periods than the experimental data. Between the 0.005 s and 0.1 s numerical results, the elevations on the foil show fairly good agreement other than the first trough.

The pressure coefficients were calculated according to Equation (5.2), where p is the local pressure on the foil surface and p_∞ is the hydrostatic pressure from the undisturbed free surface to the depth of the local pressure location.

$$C_p = \frac{p - p_\infty}{\frac{1}{2}\rho_\infty V_\infty^2} \tag{5.2}$$

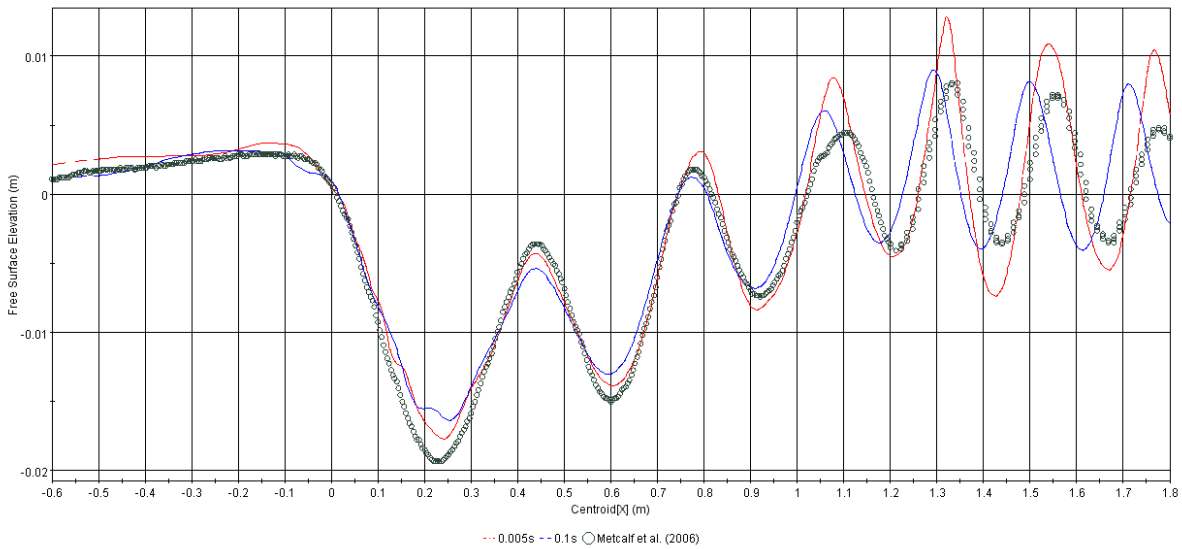

Figure 5.9: Comparison of the free surface profile at Y=0.25 m between time steps of 0.005 s and 0.1 s, and experimental results

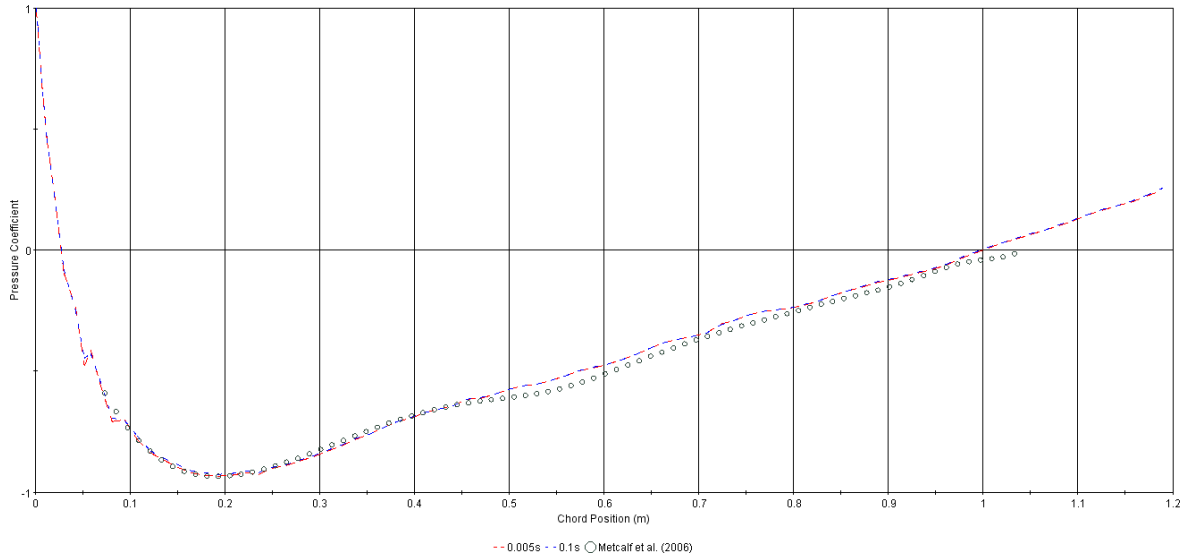

Figure 5.10: Comparison of pressure on foil surface at depth $Z = -0.1728m$ between time steps of 0.005 s and 0.1 s, and experimental results

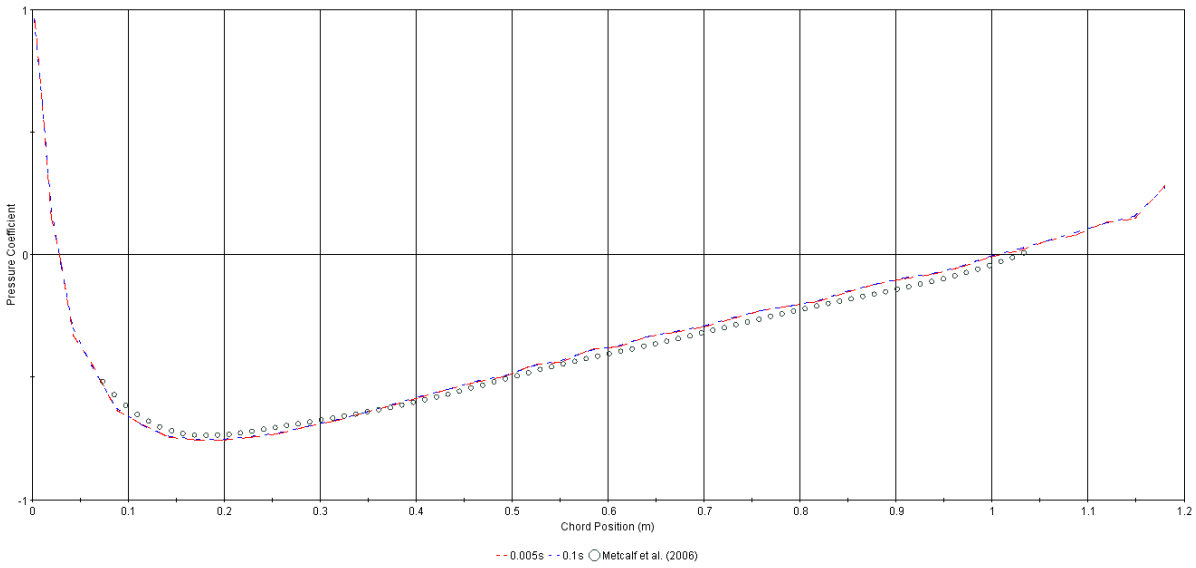

Figure 5.11: Comparison of pressure on foil surface at depth $Z = -1.11648m$ between time steps of 0.005 s and 0.1 s, and experimental results

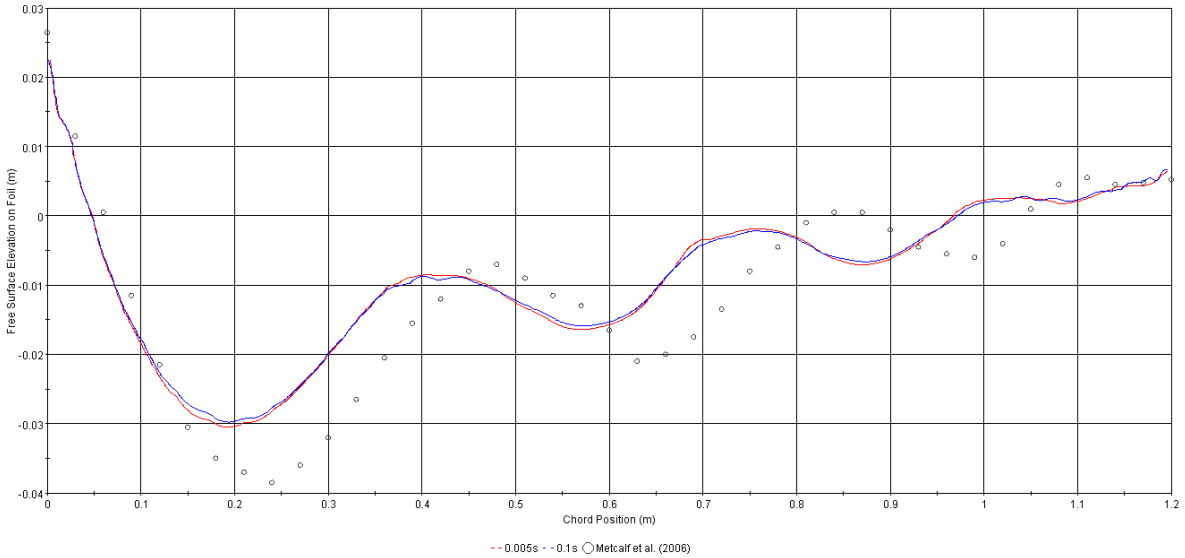

Figure 5.12: Comparison of free surface elevations at Y=0.25 *m* between time steps of 0.005 *s* and 0.05 *s*, and experimental results

5.3.2 Time Step Independence

The original mesh from Section 5.1.1, which was run with a time step of 0.005 *s*, was run a second time with a time step of 0.05s in order to see if the increased mesh resolution would allow for time step independent solution. Based on the results presented in Table 5.1 and Figure 5.13, it would indeed appear that the CD-Adapco guidelines result in a mesh that can generate a time step independent solution. The agreement of the far field free surface elevation is not perfect, but shows significantly less sensitivity than was found in the initial KCS results. Notably, the variation in the far field elevation has no influence on the drag prediction.

Compared to the 4.67 million cell mesh, which must be run at 0.005 *s* in order to generate a solution of equivalent accuracy, the mesh size is increased by 86% but the time step reduction by a factor of 10 led to a significant reduction in computational time of 78%.

Table 5.1: Comparison of drag coefficient and free surface extrema for a mesh of 8.71 million cells, showing time step independent results

Time step (s)	Cell Count	C_D Total	Min Elev. (m)	Max Elev. (m)	Core hours
0.005	8716057	0.0115	-0.03094	0.024443	768
0.05	8716057	0.0115	-0.03094	0.024443	91

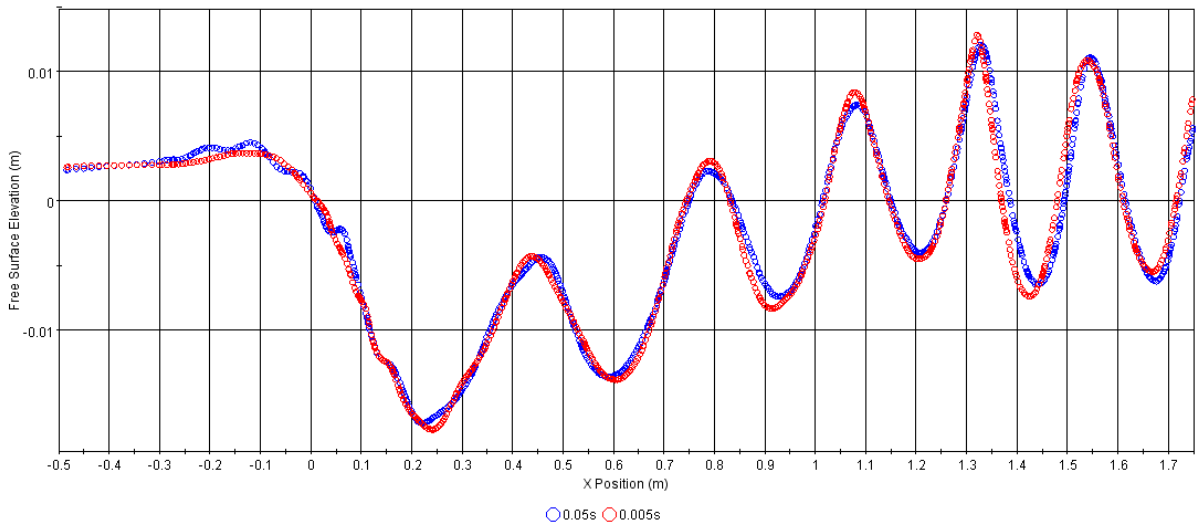

Figure 5.13: Comparison of free surface elevations on foil surface between time steps of 0.005 *s* and 0.1 *s*, for a mesh of 8.71 million cells, showing time step independence

5.4 Domain Symmetry

The assumption of a fully symmetric flow about a symmetric body is not always valid, especially when there are regions of separation around the body. Previous experience has also shown that the symmetry plane can be the source of problems with residual convergence. In order to verify the validity of the symmetry assumption implicit in the work with the NACA 0024 foil conducted thus far, and also see if residual convergence could be improved further, the half domain mesh was mirrored and combined to create a full domain mesh with perfect symmetry about the foil center plane. It is important to note this mesh symmetry, as the degree of automation in the Star-CCM+ meshing approach can sometimes lead to an asymmetric mesh even with a symmetric body and domain, which may negatively influence the results, particularly when investigating an assumption of symmetry. The results from this investigation, for a time step of 0.005 *s* are presented in Table 5.2, where it can bee seen that the region around the leading edge is subject to a slightly higher elevation in the full domain simulation, with a corresponding increase in drag coefficient.

Table 5.2: Comparison of drag coefficient and free surface extrema for the half and full domain modelling approaches, at a 0.005 *s*

Mesh	Cell Count	C_D Total	Min Elev. (m)	Max Elev. (m)	Core hours
Half Domain	4675027	0.01155	-0.03094	0.021637	420
Full domain	9350054	0.01157	-0.03094	0.023443	819

While the difference in free surface maximum elevation is 8.3%, the difference in resistance coefficient is only 0.2%. The residual plots for the half and full domain simulations are shown in Figures 5.14 and 5.15, respectively. It can be observed that the residuals generally show good convergence of about 4 orders of magnitude, except for the air phase and, by extension, the continuity residual, with little to no observable differences in convergence between the half and full domain simulations. The regions of high air phase residuals within the half domain simulation are shown in Figure 5.16, and can be seen to be located on the inlet,

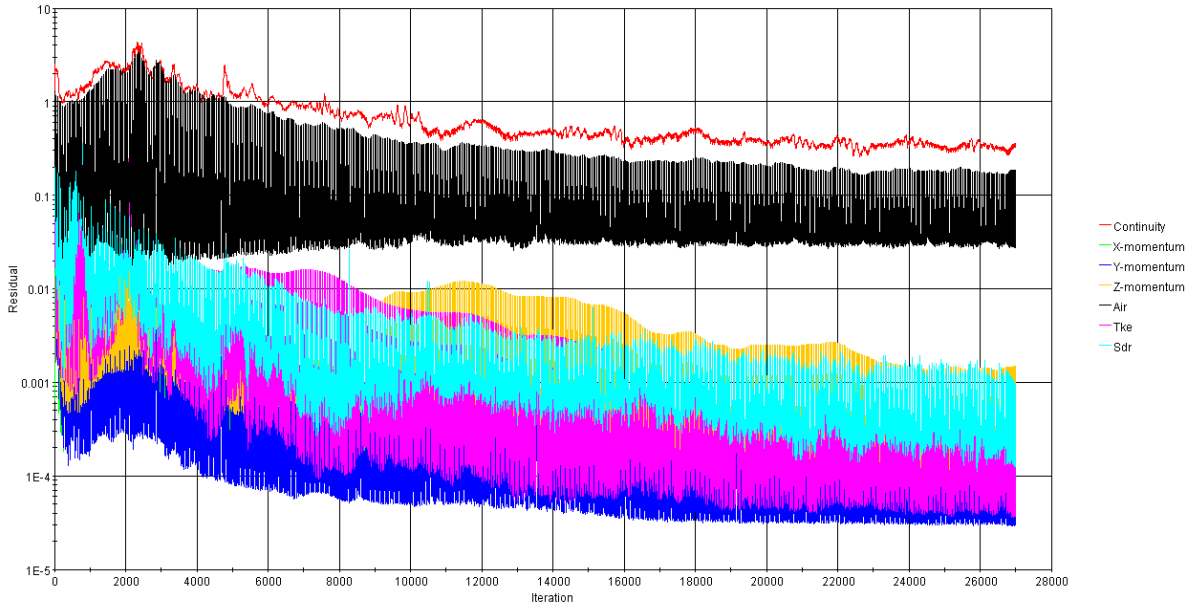

Figure 5.14: Residual history of the half domain simulation for a time step of 0.005 s and a mesh of 4.67 million cells

outlet, and symmetry plane boundaries. As the residual reported in the plot is the highest found throughout the domain, it is reasonable that the removal of the symmetry plane in the full domain case had no influence on the convergence of the air phase.

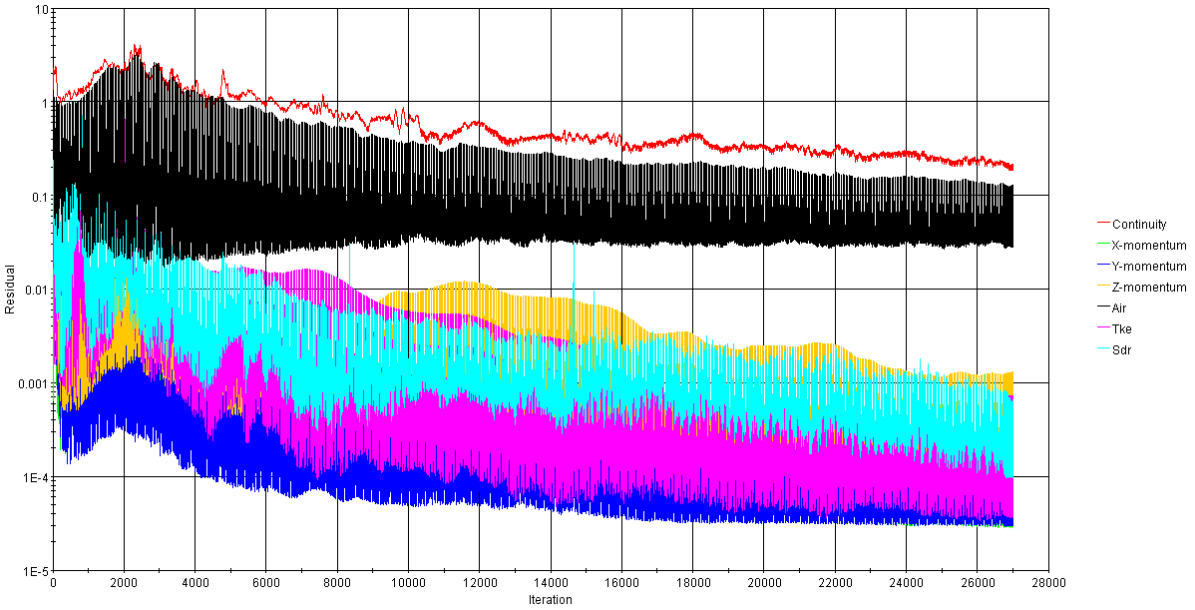

Figure 5.15: Residual history of the full domain simulation for a time step of 0.005 *s* and a mesh of 9.35 million cells

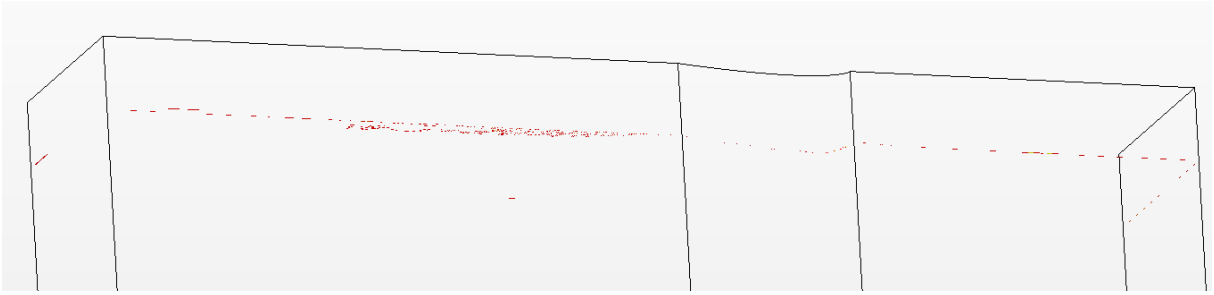

Figure 5.16: Location of high air phase residuals within the computational domain, which are found exclusively on the domain boundaries and primarily on the symmetry plane, for the half domain case at a time step of 0.005 *s* and a mesh of 4.67 million cells

5.5 Discussion

The investigation of the surface piercing NACA 0024 foil has provided an excellent case with which to delve further into findings from the 2D NACA 0012 case. In general, no sharp jump was observed in the free surface wave profile results as was found in the 2D problem, suggesting that either the issue was with the quasi 2D modelling approach, or the additional length and time scales present in the 3D case smear out any possible jumps in the numeric solvers.

As in the 2D NACA 0012 case, the time step obtained from Equation (2.7) was found to be quite conservative while the upper end of the range given by Equation (2.8) is less conservative, but still adequate to yield good results. And, also like the 2D case, a trade-off between spatial and temporal resolution could be made, with the spatial requirements for a time step independent solution being much the same. However, the intersection of the free surface mesh refinements with the prism layer near the foil surface did present some challenges, particularly as the interaction of the prism layer with the high resolution free surface refinements lead to a substantial increase in mesh count; in general, over 70% of the mesh cells were located the free surface region. The result was a cell count which, for a normal half domain ship problem, was quite high at 8.71 million cells for the time step independent mesh.

The steep, short waves created by the bluff NACA 0024 profile offered limited options for testing the aspect ratio limits in the 3D case, with an aspect ratio of 4 being the highest possible to test before inadequate resolution per wavelength began dominating the results. However, the aspect ratio of 4, and the associated 30 cells per wavelength, proved acceptable, substantially lowering the previous minimum wavelength resolution of 58 cells tested in the NACA 0012 case. This suggests that a mesh of lower resolution than previously thought can, when combined with adequate time step resolution, yield good results. This is quite an important consideration as, although the time step independent mesh proved to be the most computationally efficient approach in the case, the high mesh count resulting from the interaction between the prism layer and the free surface refinements mean that in the general case of a body with a large perimeter penetrating the free surface generating a mesh of sufficient resolution to achieve time step independence may not be practical or possibly even feasible.

Prediction of the free surface elevation on the body was found to be poor when compared with experimental values. Comparison of pressure on the body surface showed the region influenced by the poor free surface prediction to be limited to very near the free surface, indicating that flow around the aft part of the foil, which is of significance to the development of the nominal wake, is accurately predicted over the the vast majority of the foil span. The value of drag coefficient showed strong correlation to the surface elevation on the foil, but very little correlation to the far field wave elevation, indicating that the far field wave elevation has little direct influence on the drag prediction.

Chapter 6

KCS Vessel

The case of the KCS vessel at model scale is revisited in this chapter, in order to verify and validate the applicability of the findings from the 2D NACA 0012 case and the surface piercing NACA 0024 foil case. The simulation results are compared against experimental data for drag coefficient, residual coefficient, and hull surface pressure in the stern region published by Tsukada et al. (2000), and free surface elevation experimental data published by Kim et al. (2001).

The simulations with the KCS vessel were completed with Star-CCM+ version 9.02.007.

6.1 Problem Setup

The computational domain was kept as small as possible, accounting for the need to avoid having the boundaries influence the flow around the vessel, in an effort to keep the mesh cell count to a reasonable level. The free surface damping function was enabled on the inlet, outlet, and side boundaries, with a damping length of 6 m (two wavelengths). These simulations do not include appendages such as the rudder or bilge keels.

The inlet and outlet boundaries are, as in previous cases, set to velocity inlet and pressure outlet conditions, respectively, and a symmetry plane is applied on the vessel centerline. In contrast to previous cases, the upper, lower, and side boundaries are also modelled as velocity inlets with the same conditions for pressure and velocity as the inlet boundary. This is an approach used in a number of CD-Adapco tutorials for free surface flow around ships, with the intent being to represent the far field boundary conditions in a more physically meaningful way than a slip wall or symmetry plane. The location of the boundaries with respect to the reference system are given in Table 6.1

The reference system is centered at intersection of the vessel midship, centerline, and the undisturbed free surface, as shown in Figure 6.1. The x-axis is aligned parallel to, and in the direction of, the mean free stream velocity. The z-axis is oriented normal to the undisturbed free surface and positive upwards. The y-axis is oriented to give a conventional right handed system. This reference frame matches that used in the experimental free surface data.

The Courant number limits were increased for all of these simulations with the KCS vessel, with the lower and upper limits set to 40 and 50, respectively. These limits were generally

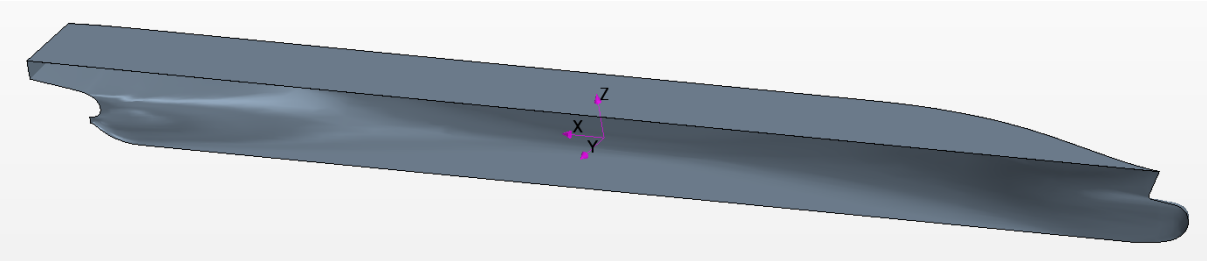

Figure 6.1: Reference system used in KCS vessel simulations

acceptable, but for several isolated sliver cells in the region near the hull at the coarsest time step. The simulation time required for convergence of the solution was found to be 140 s for the 0.05 s time step simulations, which reached a steady result, while the finer time step simulations required 200 s of simulation time to reach a stably oscillating state for the force coefficients.

6.1.1 Meshing

In order to accommodate the limitations of the Trimmer mesher, which can only increase or decrease mesh resolution by factors of 2, a slightly different approach to determining the characteristic mesh parameters was taken in comparison to the previous cases. Beginning with the maximum wave amplitude and the transverse wave length (see Table 6.1), and the intent to create a mesh, expected to be time step independent, of 20 cells per wave amplitude and 80 cells per wavelength, it was found that the cell height refinement (Z direction) was the smallest and thus limiting dimension. Selecting a cell aspect ratio to yield as close to, but not under, 80 cells per wavelength resulted in a value of 8, giving 128 cells per wavelength. The mesh base was then determined by multiplying the cell height by an appropriate power of 2 to get a size comparable to, but not exceeding, the previously used value of 0.25 m, such that the refinement sizes in the free surface region would be exactly as desired rather than the nearest approximation that the Trimmer mesher was capable of, with the result being 0.018768 m. The near wall prism mesh consists of 5 layers and is configured such that wall functions are used, with a target y^+ of 50 and the resulting wall distance calculated according to Equation (2.9).

The region around the hull is subject to several mesh refinements. The bow and stern regions have the finest resolutions, while the entire hull is enclosed in a mesh refinement volume. Unlike previous work, this refinement enclosing the entire hull is tapered in two steps to facilitate a smoother transition to the coarser base volume mesh. This smooth transition is further helped by the smaller base mesh size used in this work compared to previous efforts which used a a base mesh size of 0.25 m.

As in the previous cases, a mesh refinement block with refinements normal to the free surface extends throughout the computational domain, with a thickness approximately 10% greater than the maximum wave amplitude found in previous investigations. A second refinement block approximately 10% thicker than the first, with a coarser refinement, is used to taper the mesh transition more gradually. The refinement parallel to the free surface, shown in Figure 6.2, features a Kelvin angle (19.28°) leading edge, with a maximum width of 2.5 m and an overall length of 20.5 m, beginning 0.13 m upstream of the forward perpendicular

Table 6.1: KCS Vessel simulation parameters and relevant characteristics

General Domain Parameters	
Vessel L_{PP}	7.2786 m
Mesh base size	0.018768 m
Boundary Positions	
Inlet	$-2.5\,L_{PP}$
Outlet	$4.5\,L_{PP}$
Side	$-2.5\,L_{PP}$
Top	$1.0\,L_{PP}$
Bottom	$2.0\,L_{PP}$
Wave Parameters	
Wave length	3 m
Max amplitude	0.117 m
Initial Free Surface Refinements	
Cells per wave amplitude	20
Cell height	0.00293 m
Aspect ratio	8
Cell length	0.02346 m
Cells per wave length	128

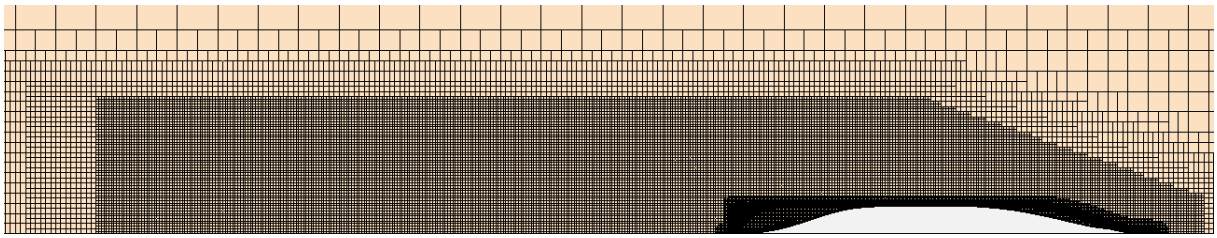

Figure 6.2: Mesh refinement blocks parallel to free surface for KCS vessel

with a width of 0.64 m, and is created using three blocks in order to better taper the cell size transition to the coarse base volume mesh.

Generating a mesh based on the above parameters, which was anticipated to yield a time step independent solution, proved incredibly demanding, requiring over 30 GB of system memory and resulting in a mesh of just under 30 million cells. A solution was not obtained for this mesh due to the extremely highly computational demands associated with such a large mesh. Halving the mesh resolution in the free surface region, to 10 cells per wave amplitude and 64 cells per wavelength, while keeping the rest of the parameters the same, resulted in a much more manageable starting point with a mesh size of 3.2 million cells.

6.2 Time Step Dependence

Based on the findings with the NACA 0024 case, it was not expected that the initial mesh, with it's resolution of 10 cells per wave amplitude and 64 cells per wavelength, would yield a time

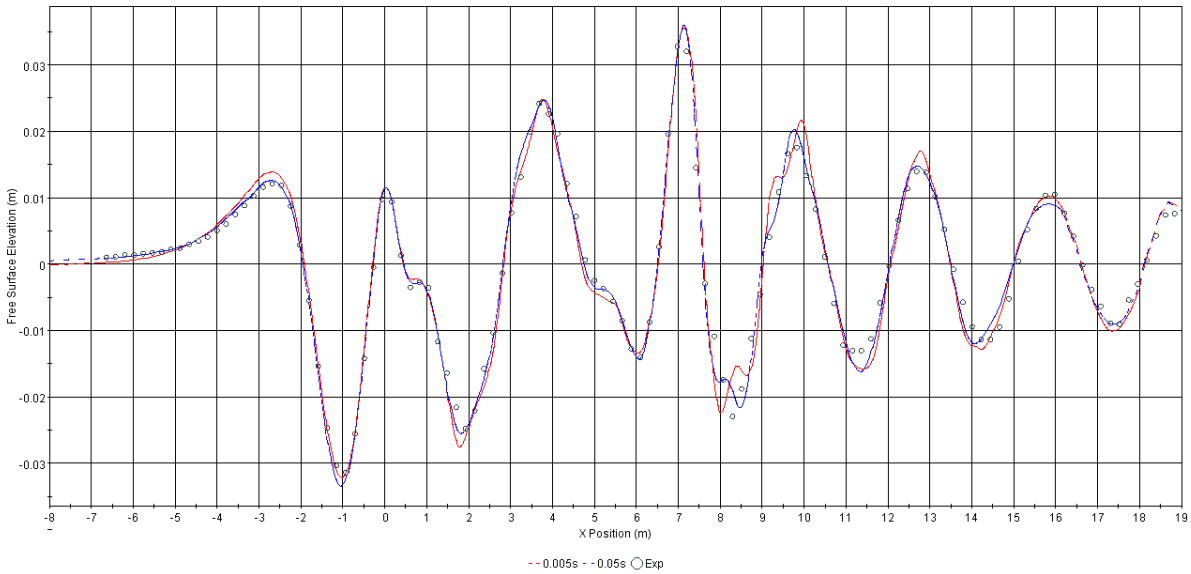

Figure 6.3: Comparison of free surface elevations at a longitudinal cut $y = -0.1509L_{PP}$ off the vessel centerline at time steps of 0.005 s and 0.05 s, and a cell aspect ratio of 8, with experimental data

step independent solution. Thus, an investigation was undertaken with the initial 3.2 million cell mesh at time steps of 0.005 s, 0.01 s, and 0.05 s. The first two values were selected based around the values calculated from Equations (2.7) and (2.8), which yielded 0.00444 s and $0.0136 - 0.0068$ s respectively, while the final one was selected as a substantially coarser step intended to push the limits of any time step sensitivity present in this configuration.

Unlike previous cases, the time step was found to have quite a significant influence on the convergence rate of the simulation. The 0.05 s simulation required 140 s of simulation time, with both the residuals and force coefficients showing no further time dependency. The 0.01 s and 0.005 s cases required 200 s of simulation time to reach a stably oscillating convergence of the force coefficients, while the residuals continued to show a gradually decreasing trend with time. Given the high computational costs, and the oscillating force coefficients, it was not deemed worth using further simulation time to investigate what values the residuals ultimately converged to. This indicates that there is more instability in the KCS case than in the previous NACA foil cases, with time scales that are not being resolved by the 0.05 s time step.

The elevation of the free surface at a longitudinal cut $y = -0.1509L_{PP}$ off the vessel centerline is shown in Figure 6.3, while the free surface elevation on the ship hull is shown in Figure 6.4, for time steps of 0.005 s and 0.05 s, as well as showing the experimental data. The resistance data for all three time steps, and the experimental results, are listed in Table 6.2, where it can be observed that the drag components show negligible sensitivity to the time step. The free surface elevation on the hull shows a very minor time step sensitivity, but clearly not sufficient to significantly influence the drag results, while the far field wave elevation shows slightly increased time step sensitivity yet again. However, compared to the results shown in Figure 1.1, the time step sensitivity of the far field of these results are orders of magnitude smaller while the time step difference is five times larger. For the purposes of this work, this mesh is deemed to yield time step independent results.

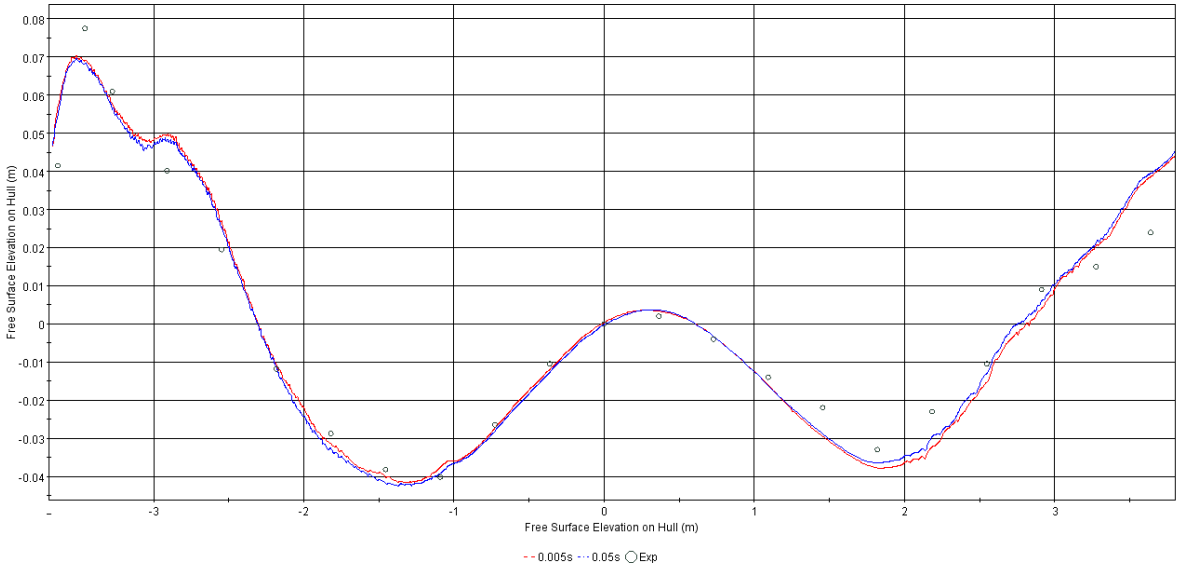

Figure 6.4: Comparison of free surface elevations on the hull of the KCS vessel at time steps of 0.005 s and 0.05 s, and a cell aspect ratio of 8, with experimental data

Table 6.2: Comparison of results for KCS vessel at different time steps, mesh aspect ratio of 8

Mesh Count	Time Step	C_D Total	C_D pressure	C_D friction	Core hours
3267888	0.05	0.00341	0.000644	0.00277	162
3267888	0.01	0.00341	0.000650	0.00276	1107
3267888	0.005	0.00341	0.000650	0.00276	2376
Experimental Values					
		0.00352	0.0006888	0.00283	
Percent Error					
		−3.10	−5.63	−2.48	

The agreement between the experimental and numerical results for the far field wave elevations are very good, amongst the best obtained in this work. But, as in the NACA 0024 case, the agreement on the body surface is substantially poorer, leading to an underprediction of pressure drag term (typically referred to as the residual component or C_r for ship cases). It is interesting to note that the frictional resistance component is also underpredicted. However, the 3.1% underprediction of the total drag is comparable or better than the underprediction of 4.86% reported by Enger et al. (2010) for the KCS case with rudder, using Star-CCM+ and the k-ω SST turbulence model.

6.3 Aspect Ratio

The nature of the free surface wave pattern in this case, being much less steep than that of the NACA 0024 case, lends itself much more readily to investigating higher aspect ratio mesh cells in the free surface refinement region. To that end, the number of cells per wavelength in the initial mesh was halved, to 32, which in turn increased the cell aspect ratio to 16. The resulting mesh cell count was 1.8 million cells. It was not deemed necessary to investigate higher aspect ratios as the NACA 0012 results already suggest they should be avoided and, more practically, if the cell count were to be reduced further, reducing cell count per wave amplitude should be the next step as this is expected to have a much better trade-off in terms of cell count versus impact on simulation accuracy.

The results for the aspect ratios of 8 and 16 are compared in Figures 6.5 and 6.6, for the far field wave elevation and elevation on the hull, respectively, at a time step of 0.05 s. The agreement between the two meshes in the far field is good, while the agreement on the hull is almost perfect. This agreement is reflected in the drag coefficient values, as shown in Table 6.3. Perhaps the most surprising result, indicated by the drag results and confirmed by the far field free surface elevations shown in Figure 6.7, is that the 1.8 million cell mesh, with 10 cells per wave amplitude and 32 cells per wavelength, is also providing a time step independent solution.

Table 6.3: Comparison of results for KCS vessel at different time steps, mesh aspect ratio of 16

Mesh Count	Time Step	C_D Total	C_D pressure	C_D friction	Core hours
1842388	0.05	0.00341	0.00065	0.002759	99
1842388	0.01	0.00341	0.00065	0.002761	636
1842388	0.005	0.00341	0.00065	0.002761	1296
3267888	0.005	0.00341	0.00065	0.002761	2376

As with the initial mesh, the 1.8 million cell mesh required substantially more simulation time for convergence of the 0.01 s and 0.005 s, again at 200 s, compared with the 140 s required for the 0.05 s time step.

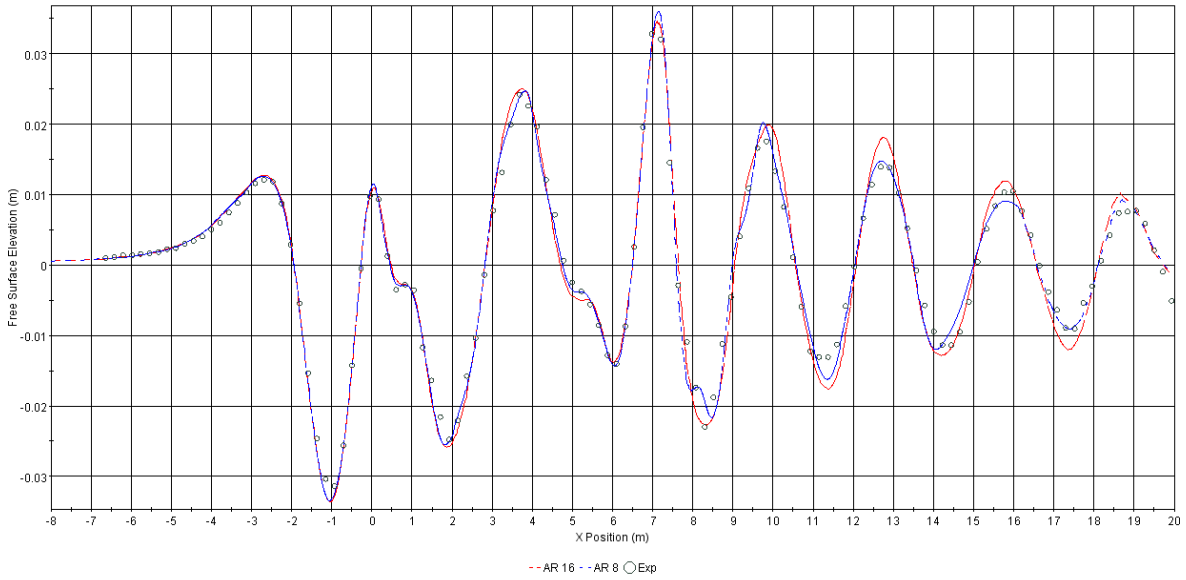

Figure 6.5: Comparison of free surface elevations at a longitudinal cut $y = -0.1509L_{PP}$ off the vessel centerline, for mesh aspect ratios of 8 and 16, with experimental data

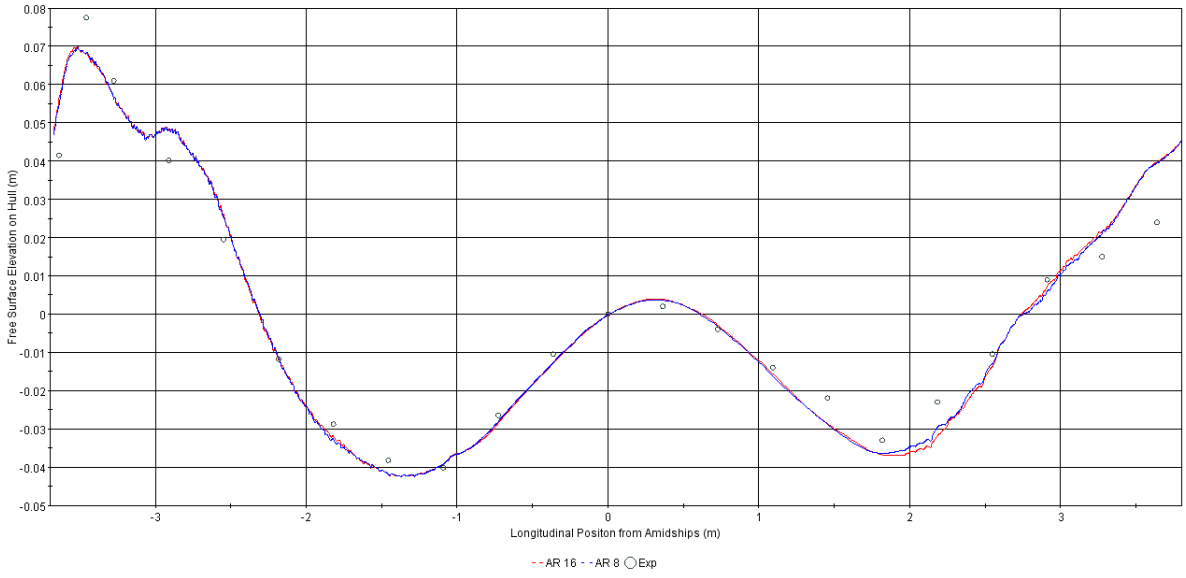

Figure 6.6: Comparison of free surface elevations on hull of the KCS vessel, for aspect ratios of 8 and 16, with experimental data

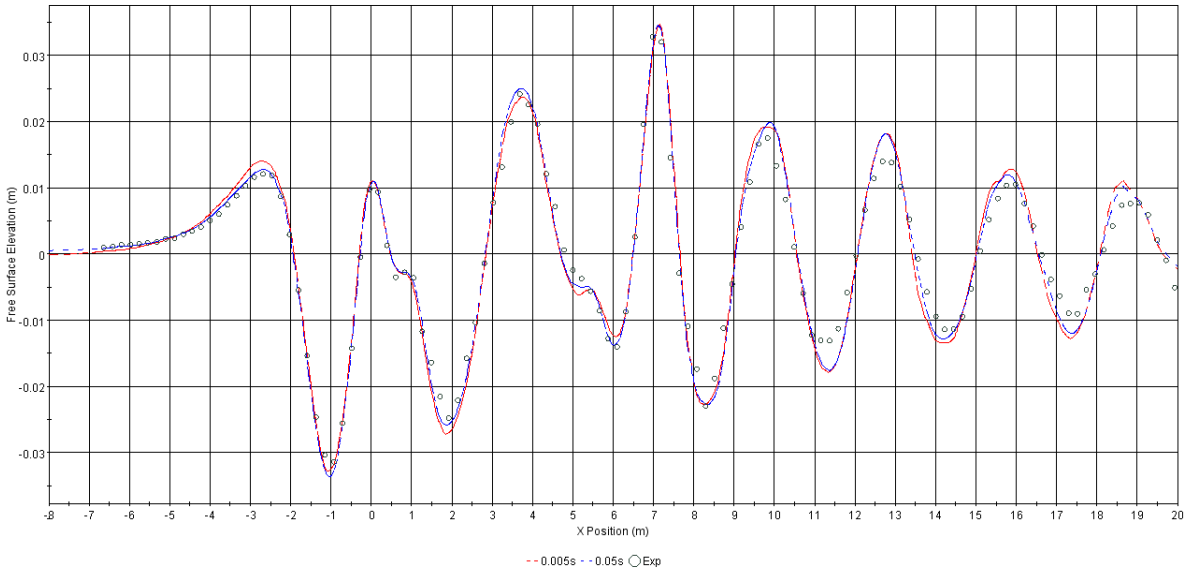

Figure 6.7: Comparison of free surface elevations at a longitudinal cut $y = -0.1509 L_{PP}$ off the vessel centerline at time steps of 0.005 s and 0.05 s, and mesh aspect ratio of 16, with experimental data

6.4 Hull Surface Pressure

The numerical and experimental pressures on the surface of the hull in the stern region, at longitudinal cuts at $Z = -0.089\,m$ and $Z = -0.279\,m$, are compared in Figures 6.8 and 6.9, for the 1.8 million cell mesh at a time step of 0.05 s. The pressure coefficient is calculated according to Equation (5.2), as detailed in Section 5.3.1. The agreement between the experimental and numerical results are very good both in the vicinity of the free surface and closer to the keel, indicating that both the free surface and turbulence models are adequately capturing the relevant flow features in the vicinity of the hull.

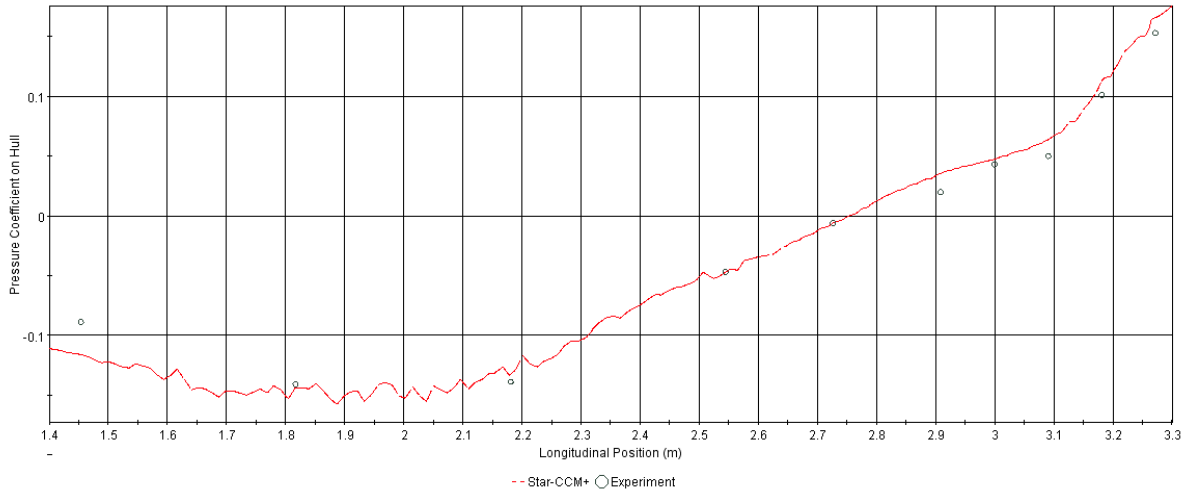

Figure 6.8: Pressure coefficient on the hull surface at a longitudinal cut $Z = -0.089\,m$ for the 1.8 million cell mesh at a time step of $0.05\,s$, compared with experimental data

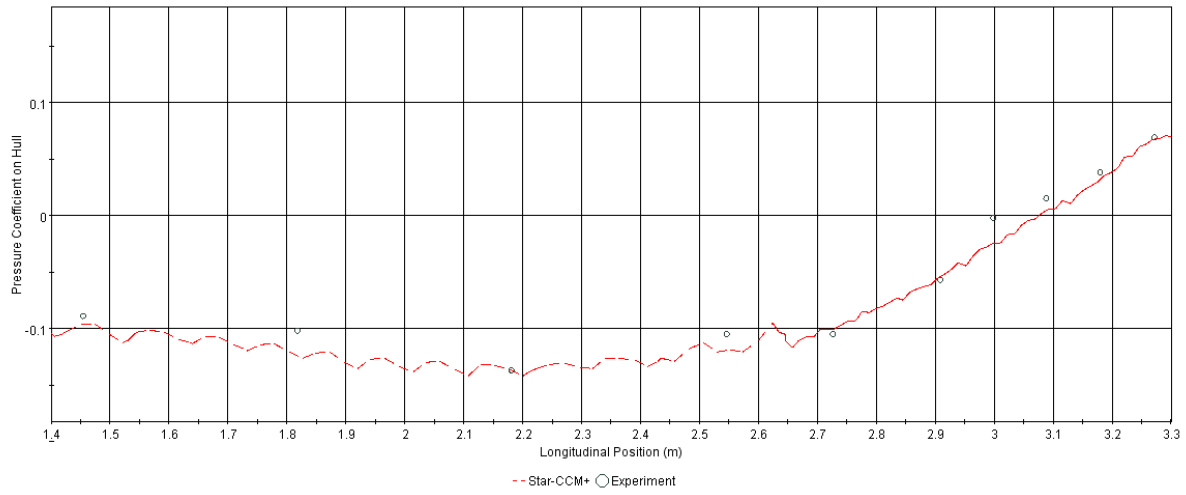

Figure 6.9: Pressure coefficient on the hull surface at a longitudinal cut $Z = -0.279\,m$ for the 1.8 million cell mesh at a time step of $0.05\,s$, compared with experimental data

6.5 Residual Convergence

One of the issues identified in Chapter 1 with the inital KCS simulation efforts was poor residual convergence. The residual plots for the results presented in this section are substantially improved, with an example shown in Figure 6.10 for the 1.8 million cell mesh with 10 cells per wave amplitude and 32 cells per wavelength, compared to the example shown in Figure 1.2. In spite of the improvements, the residuals still do not display the desired convergence levels of $3-4$ orders of magnitude, with the air phase residual (which influences the continuity residual) showing the worst convergence, as has been the case throughout the simulations undertaken in this work. The worst air residuals, and indeed the worst residuals for all the parameters shown in Figure 6.10, are found along the domain boundaries, particularly on the symmetry plane downstream of the ship hull, as in the NACA 0024 case.

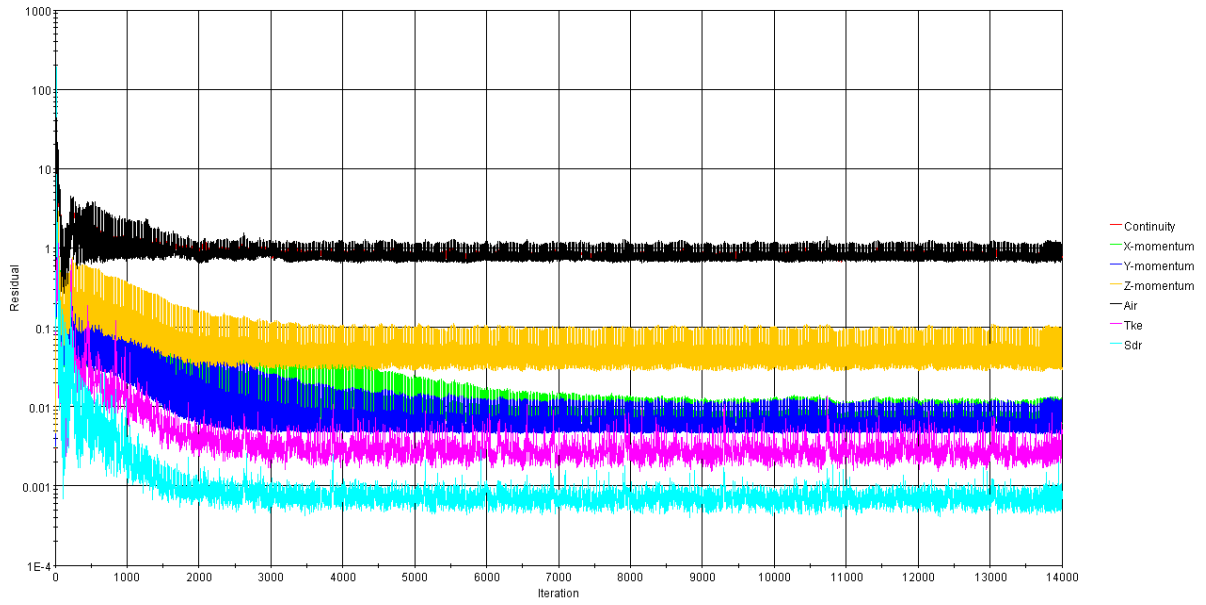

Figure 6.10: Residual convergence for a mesh with an aspect ratio of 16, 1.8 million cells, and time step of 0.05 *s*

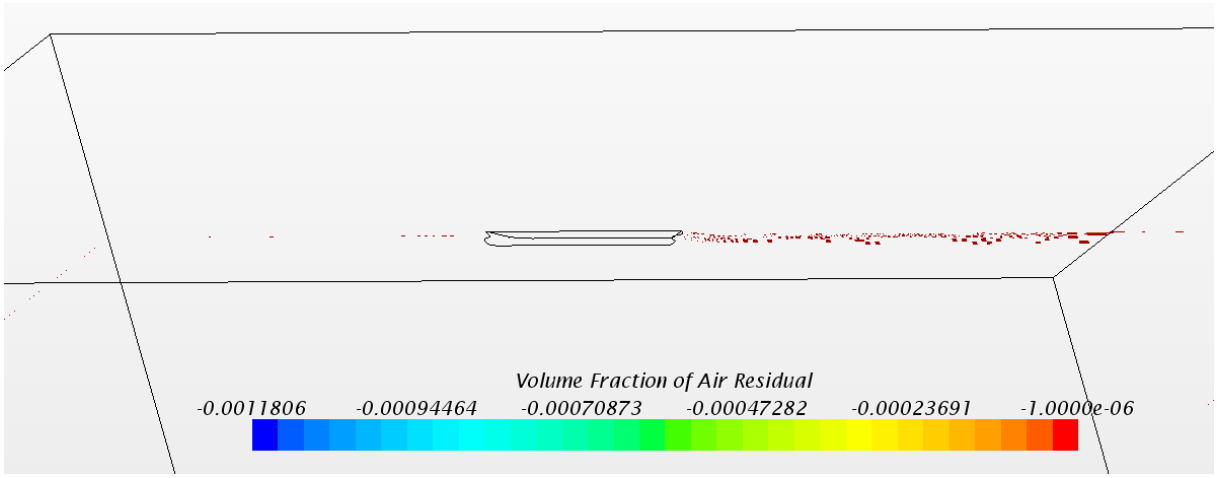

Figure 6.11: Location of worst air phase residuals for KCS simulation, found exclusively on the domain boundaries and primarily on the symmetry plane downstream of the ship hull

6.6 Discussion

The revisit of the KCS vessel has shown that some, but not all, of the lessons learned with the two NACA cases are applicable to the ship problem. The mesh resolution originally expected to be required for time step independence, with 20 cells per wave amplitude and 128 cells per wavelength proved to be far to computationally demanding to be feasible at a cell count of almost 30 million. However, the coarser meshes, featuring 10 cells per wave amplitude and 32 and 64 cells per wavelength, for mesh counts of 1.8 and 3.2 million cells, respectively, proved to provide adequate resolution to yield a time step independent solution for this case. This is substantially lower resolution for time step independence than was found in the previous cases, which is somewhat surprising given that the ship case, with the interacting bow and stern waves, presents perhaps the most complicated free surface deformation to capture. One possible explanation, when looking at the two surface piercing cases of the NACA 0024 foil and the KCS vessel, is that the wave generated by the KCS vessel is much less steep, with wavelength to height ratio of $25.6:1$, compared to $6.5:1$ for the NACA 0024 foil. Indeed, the NACA 0024 case is clearly right on the edge of breaking, well below the normal threshold of $8:1$ given for a linear wave, and with such a steep slope, the flow in the free surface region is much less orthogonal to the hexahedral mesh than is the case for the KCS vessel.

In general, no new limitations in terms of resolution have been found with this case, other than the heavy cost of the interaction between the boundary layer mesh and the free surface refinements for a body that presents a large perimeter to this intersection region. The 30 cell per wavelength limit is the same as was found with the NACA 0024 case, while the aspect ratio up to 16 is in agreement with the findings from the NACA 0012 case, and the resolution of $10-20$ cells per wave amplitude is in agreement with both cases. As in the previous cases, the CD-Adapco (eq. (2.7)) time step recommendations proved to be very conservative, while the ITTC time step recommendations (eq. (2.8)) also, in contrast to previous cases, proved to be very conservative even at the coarse end of the suggested range.

The overall agreement between the experimental and numerical results is excellent. The free surface elevation on the hull shows the most substantial discrepancy, with a corresponding error in the vessel drag coefficient. This error is however slightly better than that reported by

Enger et al. (2010) for the KCS case with rudder, using Star-CCM+. The pressure on the hull in the stern region is in very good agreement, indicating that in spite of the discrepancies in free surface elevation and drag coefficient, the physics of the flow are captured well enough to provide a good starting point for investigation of the nominal wake behind the ship.

The residual behaviour remains somewhat less than ideal, with only $2-3$ orders of magnitude convergence for most residuals and less than one for the air phase residual. However, in comparison to earlier efforts, the residual behaviour is very much improved. In addition, viewing the location of the worst residuals within the domain show them to be located almost exclusively on the boundaries, and on the symmetry plane in particular, with the vast majority of the flow field showing convergence more in keeping with the desired 4 orders of magnitude or better.

Chapter 7

Summary

In general, the primary objectives outlined for this thesis work have been satisfied. The theoretical investigation of free surface modelling, and the systematic investigations conducted with the benchmark cases, led to the modification of some solver parameters and a modelling approach for free surface flows which yields good results at an acceptable computational cost. The acquired knowledge has been applied to the KCS vessel, with a substantial improvement in the simulation results having been obtained, including improved residual convergence.

The findings from the investigations of the preceding chapters are summarized in the following sections and, where possible, guidelines based on these findings are formulated for general application to modelling of free surface flows with the Star-CCM+ software package.

7.1 Modelling and Problem Setup

In general, the default Star-CCM+ settings for the segregated volume of fluid model are able to produce good results, with the notable exception of the default Courant number limits in the VOF model, which must be increased for steady flow problems in order to achieve a good solution in a computationally efficient manner. The level at which these limits are increased to has no bearing on the results, as long as they are higher than the peak Courant number within the free surface region, ensuring the use of the HRIC discretization scheme for the volume of fluid function.

The influence of the symmetry plane on the simulation results was investigated for the NACA 0024 case, and found to have very little influence on the results or residual convergence. Given the good agreement between the experimental and numerical data for the KCS case, this symmetry assumption also appears to be valid for the resistance and free surface prediction in spite of the increased unsteadiness in the stern region of the KCS case compared to the NACA 0024 case. It remains uncertain whether the symmetry assumption would remain valid for the prediction of nominal wake in the KCS case, where any instabilities in the stern region have greater opportunity to propagate over a larger region, including across the vessel centerline.

7.2 Spatial Resolution

The minimum requirements for mesh resolution in the free surface region were established with the 2D NACA 0012 case, elaborated further with the 3D NACA 0024 and KCS cases, and found to be quite consistent throughout the series of investigations. Theses requirements are summarized in Table 7.1.

Table 7.1: Minimum mesh resolution requirements in the free surface region for obtaining accurate results

Parameter	Value
Cells per wave amplitude	8 or more
Cells per wavelength	30 or more
Cell aspect ratio	16 or less

If reference data is not available prior to commencing the simulations from which an expected wavelength and amplitude can be obtained, the wavelength can be estimated with Equation (5.1). Unfortunately, no simple method of estimating wave amplitude has been identified in the course of this work; either a preliminary simulation with very coarse resolution or a potential flow calculation is likely to be the best starting point.

All the cases investigated afforded the possibility of generating a mesh of sufficient resolution that the solution was, within reasonable limits, independent of time step. This was, in all cases, found to be the least computationally demanding approach to obtaining good results. Unfortunately, the requirements for generating such a mesh varied much more from problem to problem than the minimum resolution requirements. The cell aspect ratio limit of 16 or less applied throughout the cases, but the number of cells per wave amplitude and wavelength required varied from case to case and are summarized in Table 7.2. It is important to note that the resolution target per wave length for the NACA 0024 case was 80, and the resulting 120 was simply a result of the Trimmer mesher quantisation limitations. It is expected, but not confirmed, that a lower resolution, such as 80 cells per wavelength, would in fact be adequate for time step independence.

Table 7.2: Mesh resolution requirements for time step independent solution for the NACA 0012, NACA 0024, and KCS vessel cases

2D NACA 0012 Foil	
Cells per wave amplitude	17
Cells per wavelength	85
NACA 0024 Foil	
Cells per wave amplitude	20
Cells per wavelength	120*
KCS Vessel	
Cells per wave amplitude	10
Cells per wavelength	32

In general, the Star-CCM+ mesh resolution recommendations seem to be a good starting

point for obtaining a time step independent mesh. Unfortunately, due to the incredibly high mesh count resulting from trying to implement these recommendations for the KCS vessel case, it is simply unfeasible to recommend this even as a conservative option for the flow around a ship. Leaving the 2D NACA 0012 case aside, as many of the characteristics of the results obtained from that case are of a different nature to the pair of 3D flow problems investigated, the spatial resolution requirements correlate very strongly to the maximum wave slope; that is, a short, steeper wave system, such as that generated by the surface piercing NACA 0024 foil, requires higher resolution than the longer, gentler waves generated by the KCS vessel. Considering the effects of a steep wave system on the orthogonality of the mesh to the flow, reducing it substantially, this hypothesis makes even more sense. However, when including the results from the NACA 0012 foil, the requirements for a time step independent mesh must be deemed somewhat inconclusive. Investigation of an additional hull, ideally of fuller dimensions than the KCS vessel, would potentially allow a more conclusive assessment to be reached.

7.3 Temporal Resolution

Throughout the test cases investigated in this work, the time step recommendation given by CD-Adapco in Equation (2.7) has proven significantly more conservative than required for good results. The nature of the equation, with decreasing time step as the number of cells per wavelength is increased, implies the satisfaction of some sort of Courant number limit. Whether this is to work in conjunction with the default Courant number limits in the VOF model, or to satisfy a more general requirement for time varying free surface simulations is unclear. It is clear however, that the philosophy behind Equation (2.7) is not particularly appropriate for the essentially steady ship towing test class of simulations

The time step recommendation provided by the ITTC, given in Equation (2.8), covers a range of acceptable values. The fine end of the range was found to be comparable to the CD-Adapco for the cases investigated here, being again more conservative than necessary. The coarse end of the range was found be be a good starting point for the time step dependent meshes, always recommending an adequate time step for obtaining good results without adding excessive computational demands. When used as in this thesis work, where the characteristic length is taken to be the wavelength of the transverse wave system, the philosophy behind Equation (2.8) makes more sense for steady free surface flows: flows with longer wave periods are recommended a larger time step. For marine applications, wave with longer periods are generally less steep with lower gradients and larger length and time scales in comparison to short period waves. As such, based on the findings obtained during this thesis work, the ITTC guideline is simplified to provide the recommended time step, for the free surface region around a body (considerations such as substantial separation or vortex shedding are not accounted for), given by Equation (7.1):

$$\Delta t = 0.01 \frac{L}{U} \tag{7.1}$$

Where L is the wavelength of the transverse wave system, and U is the mean free speed velocity. This recommended time step should, in conjunction with the recommended minimum spatial resolution, ensure acceptable results are obtained for the free surface. Where a time

step independent mesh is used, the time step from Equation (7.1) can safely be increased by at least a factor of $2-4$.

Some care must be used for low Froude number cases, as both the wave period of the system created by the ship and the relative contribution of the wave system to the drag and nominal wake reduce with decreasing Froude number, and eventually the decreasing time step suggested by Equation (7.1) will result in high computational costs for no appreciable improvement in the simulation results.

7.4 Residual Convergence

The residuals throughout the simulations undertaken here showed acceptable convergence, in general, with the exception of the air phase residual. Although the desired $3-4$ orders of magnitude reduction in the residuals was never achieved, the momentum and turbulence model residuals showed convergence of approximately 3 orders of magnitude, with the peak values always found on the domain boundaries, where their influence on the solution is expected to be small.

The air residual never showed any significant degree of convergence, with the continuity residual being influenced by this and never showing good convergence either. Given the location of the worst of the air phase residuals, primarily downstream of the body, near the free surface, and on the symmetry plane boundary, it would be reasonable to assume that some unsteadiness in flow is either interacting poorly with the symmetry boundary or the enforcement of the HRIC scheme is leading to a sharp interface in a region where there is not adequate resolution to capture the flow properly. However, these theories fly in the face of the fact that the air residual behaved exactly the same in the purely steady 2D NACA 0012 case as in the other cases. Given that the air phase has negligible effect on the overall simulation results, the issue was not deemed worth further investigation.

7.5 Further Work

The main question left unresolved is the required mesh resolution for a time step independent solution of the flow around a ship hull. Indications from the KCS case are that, for a wave system of modest slope, the requirements are much lower than the two foil cases would suggest. It seems prudent then, to extend the time step dependency investigation to include at least one more ship hull, ideally of blunter proportions than the KCS vessel in order to generate a wave system with a steepness in between that of the KCS and NACA 0024 cases. For this purpose, the well investigated KVLCC ship would be an excellent candidate.

The remainder of the objectives laid out for the thesis work have been satisfied, and a good starting point for investigation of the ship nominal wake established. Such an investigation of the ship nominal wake should include a focus on turbulence models, and any possible trade-offs between wake resolution and other parameters of interest, and the validity of the symmetry plane on the vessel centerline. Given the low amount of separated flow in stern region of the KCS vessel at $Fr = 0.26$, it may be worth including another hull form that features steeper pressure gradients in order to push the capabilities of the turbulence models.

It is expected that the Reynolds Stress Model, which unlike the one and two equation turbulence models does not assume that the turbulent length scales are isotropic in nature, will perform better in such a scenario, but possibly at the cost of less accurate prediction of vessel resistance.

Chapter 8

Conclusions

The Star-CCM+ simulation software has been used to model a number of benchmark free surface flow cases, including the two dimensional submerged NACA 0012 foil, the surface piercing NACA 0024 foil, and the well investigated KCS vessel. The findings from the foil benchmark cases have permitted substantial improvement in the accuracy and convergence of the results for the KCS vessel when compared to initial studies undertaken as part of the master's project.

It has been observed that a minimum set of temporal and spatial resolutions are required to yield an acceptable numerical solution, and guidelines to ensure that these requirements are met have been formulated, including modification of the default Star-CCM+ modelling parameters for supposedly steady state free surface flows. The cause of this resolution requirement, whether meshing, modelling, or implementation based, remains unknown. As discussed in Section 3.3, there may be an issue with the VOF method not guaranteeing conservation of energy near the free surface interface, with the minimum mesh resolution requirements then ensuring an accurate enough approximation to yield acceptable results. However, with the VOF method implemented in Star-CCM+, where both phases are solved for on a co-located grid, this criticism, which was of the original implementation of Hirt and Nichols (1981) where the air phase was omitted from the solution, would appear to be less valid. Another possibility is that a minimum resolution is required to capture all the relevant spectral components making up the free surface wave system. This seems unlikely as, since the wave systems in the cases investigated here are stationary, the resolution requirements should then be purely spatial. In addition, the requirement of 30 cells or more per wavelength would suggest that spectral components as high as the 15th harmonic are of sufficient amplitude to make significant contribution to the free surface elevation.

In practical terms, identifying the source of the minimum resolution requirements is less significant than being aware that they exist, and what the requirements are. These minimum resolution requirements are fairly consistent across all the cases investigated, permitting the formulation of some basic guidelines which are expected to have fairly general applicability to modelling free surface flows with Star-CCM+.

Time step independent solutions for all of the cases investigated have been found, however the mesh resolution requirements to obtain this independence are subject to more variance from case to case than the minimum resolution requirements, and some practical limitations regarding mesh size in the ship case precludes taking the most demanding require-

ments found and using them as a general recommendation. Some additional work, focusing on investigation of additional ship cases, has been proposed with the objective of clarifying guidelines for creating a time step independent mesh for ship flow problems.

The agreement with the experimental references throughout the investigated cases have, in general, been good. The far field free surface elevations, greater than $1-2$ wavelengths from the body, were found to have little direct influence of the on the drag prediction; the elevation of the free surface on the body was found to be of much greater significance. The free surface elevation on the surface piercing bodies have shown the largest discrepancies, with an accompanying error in the prediction of the drag coefficient. However, comparison with pressure measurements on the body surfaces, which are in very good agreement in the cases where this experimental data is available, has shown that the region of influence of the inaccurate free surface prediction to be confined to a small region in the immediate vicinity of the free surface. Thus, the turbulence and free surface models appear to be resolving the flow accurately over much of the domain, particularly the aft region which is the most relevant to development of the nominal wake.

In general, an improved modelling approach for free surface flows has been elaborated, using the Star-CCM+ software, which yields improved convergence of the force coefficients and normalized residuals. As such, this constitutes a satisfactory conclusion for prediction of ship resistance and a good starting point for further investigation of the nominal wake scaling problem.

Appendix A

Piezometric Pressure Field Function

The custom field function used for calculating piezometric pressure is given below.

$AbsolutePressure-101325.0+$$Position[2]*9.81*(997.561*$VolumeFractionWater+1.181*(1-$VolumeFractionWater))

The assumptions implicit in the code as given are:

- Default coordinate system is located at the undisturbed free surface.
- Z axis is normal to free surface and positive upwards (into air phase).
- Default Star-CCM+ values are used for reference pressure, gravity, water density, and air density.

Bibliography

Ali, A. and Karim, M. (2010). NUMERICAL STUDY OF FREE SURFACE EFFECT ON THE FLOW AROUND SHALLOWLY SUBMERGED HYDROFOIL. (December):1–6.

Caretto, L., Gosman, A., Patankar, S., and Spalding, D. (1973). Two calculation procedures for steady, three-dimensional flows with recirculation. In Cabannes, H. and Temam, R., editors, *Proceedings of the Third International Conference on Numerical Methods in Fluid Mechanics*, volume 19 of *Lecture Notes in Physics*, pages 60–68. Springer Berlin Heidelberg.

Choi, J. and Yoon, S. B. (2009). Numerical simulations using momentum source wave-maker applied to rans equation model. *Coastal Engineering*, 56(10):1043–1060.

Duncan, J. H. (1982). The breaking and non-breaking wave resistance of a two-dimensional hydrofoil. *Journal of Fluid Mechanics*, 126:507 – 520.

Enger, S., Perić, M., and Perić, R. (2010). SIMULATION OF FLOW AROUND KCS-HULL. In Larson, L., Stern, F., and Visonneau, M., editors, *Gothenburg 2010 Workshop on Numerical Ship Hydrodynamics*, pages 411–416, Gothenburg.

Faltinsen, O. (1993). *Sea Loads on Ships and Offshore Structures*. Cambridge Ocean Technology Series. Cambridge University Press.

Faltinsen, O. (2005). *Hydrodynamics of High-Speed Marine Vehicles*. Cambridge University Press.

Ferziger, J. and Perić, M. (2002). Finite volume methods. In *Computational Methods for Fluid Dynamics*, pages 381–397. Springer Berlin Heidelberg.

Gillis, S. How do I setup my mesh to best capture VOF Waves. URL https://cd-adapco.secure.force.com/index/ArticleDetail?id=kA8400000008PRbCAM&type=FAQ__kav&searchTerm=vof&Product=&Type=&Faq=&_strSearchType=Basic&knowledgebase=true. Last accessed February 18, 2014.

Hirt, C. W. and Nichols, B. D. (1981). Volume of fluid (vof) method for the dynamics of free boundaries. *Journal of computational physics*, 39(1):201–225.

ITTC (2011). Recommended Procedures and Guidelines: Practical Guidelines for Ship CFD. Technical report, International Towing Tank Conference.

Kim, W., Van, S., and Kim, D. (2001). Measurement of flows around modern commercial ship models. *Experiments in Fluids*, 31(5):567–578.

Krasilnikov, V. I. (2013). Self-Propulsion RANS Computations with a Single-Screw Container Ship. In *Third International Symposium on Marine Propulsors*, number May, Launceston, Tasmania, Australia.

Krasilnikov, V. I. (2014). Numerical Modelling of Ship-Propeller Interaction under Self-Propulsion Condition. In CD-Adapco, editor, *Proceedings of the STAR Global Conference 2014*, Vienna.

Lewis, E., of Naval Architects, S., and (U.S.), M. E. (1988). *Principles of Naval Architecture: Resistance, propulsion and vibration*. Principles of Naval Architecture. Society of Naval Architects and Marine Engineers.

Löhner, R. (2008). *Applied Computational Fluid Dynamics Techniques : An Introduction Based On Finite Element Methods*. J. Wiley and sons, Chichester, 2nd edition.

Menter, F. R. (1994). Two-equation eddy-viscosity turbulence models for engineering applications. *AIAA Journal*, 32(8):1598–1605.

Metcalf, B., Longo, J., Ghosh, S., and Stern, F. (2006). Unsteady free-surface wave-induced boundary-layer separation for a surface-piercing NACA 0024 foil: Towing tank experiments. *Journal of Fluids and Structures*, 22(1):77–98.

Muscari, R. and Mascio, A. D. (2003). A Model for the Simulation of Steady Spilling Breaking Waves. 47(1):13–23.

Muzaferija, S. and Peric, M. (1999). Computation of free-surface flows using interface tracking and interface-capturing methods. *Advances in Fluid Mechanics*, 24:59–100.

Ransau, S. (2004). *Numerical Methods for Flows with Evolving Interfaces*. PhD thesis, Norwegian University of Science and Technology, Faculty of Engineering Science and Technology.

Thomas, T., Williams, J., and Leslie, D. (1992). Development of a conservative 3d free surface code. *Journal of Hydraulic Research*, 30(1):107–115.

Tsukada, Y., Hori, T., Ukon, Y., Kume, K., and Takeshi, H. (2000). Surface pressure measurements on the kcs model (sri ms no. 631) in the sri 400m towing tank. *Ship Performance Division Report No. 00±004±01. The Ship Research Institute of Japan, Mitaka, Japan*.

University of Iowa (2013). NACA24. URL http://www.iihr.uiowa.edu/shiphydro/efd-data/naca24/?doing_wp_cron=1401090621.1394209861755371093750. Last accessed March 12, 2014.

White, F. (1991). *Viscous Fluid Flow*. McGraw-Hill international editions: Mechanical engineering series. McGraw-Hill Book Company.

Zhang, Z. and Stern, F. (1996). Free-surface wave-induced separation. *Journal of fluids engineering*, 118(3):546–554.